

NDE Technology Engineering Program for Hanford DST Non-Visual Volumetric Inspection Technology – Phase II RAVIS Radiation Tolerance Test Report

August 2020

MK Murphy
KM Denslow
JF Christ
GL Carter
MS Taubman

DISCLAIMER

This report was prepared as an account of work sponsored by an agency of the United States Government. Neither the United States Government nor any agency thereof, nor Battelle Memorial Institute, nor any of their employees, makes **any warranty, express or implied, or assumes any legal liability or responsibility for the accuracy, completeness, or usefulness of any information, apparatus, product, or process disclosed, or represents that its use would not infringe privately owned rights.** Reference herein to any specific commercial product, process, or service by trade name, trademark, manufacturer, or otherwise does not necessarily constitute or imply its endorsement, recommendation, or favoring by the United States Government or any agency thereof, or Battelle Memorial Institute. The views and opinions of authors expressed herein do not necessarily state or reflect those of the United States Government or any agency thereof.

PACIFIC NORTHWEST NATIONAL LABORATORY
operated by
BATTELLE
for the
UNITED STATES DEPARTMENT OF ENERGY
under Contract DE-AC05-76RL01830

Printed in the United States of America

Available to DOE and DOE contractors from the
Office of Scientific and Technical Information,
P.O. Box 62, Oak Ridge, TN 37831-0062;
ph: (865) 576-8401
fax: (865) 576-5728
email: reports@adonis.osti.gov

Available to the public from the National Technical Information Service
5301 Shawnee Rd., Alexandria, VA 22312
ph: (800) 553-NTIS (6847)
email: orders@ntis.gov <<https://www.ntis.gov/about>>
Online ordering: <http://www.ntis.gov>

NDE Technology Engineering Program for Hanford DST Non-Visual Volumetric Inspection Technology – Phase II RAVIS Radiation Tolerance Test Report

August 2020

MK Murphy
KM Denslow
JF Christ
GL Carter
MS Taubman

Prepared for
the U.S. Department of Energy
under Contract DE-AC05-76RL01830

Pacific Northwest National Laboratory
Richland, Washington 99354

Summary

This test report provides the results of radiation tolerance robustness testing that was performed on samples of robotic components and an ultrasonic guided wave air-slot sensor that represent components/sub-systems of the Robotic Air-slot Volumetric Inspection System (RAVIS) that has been engineered for volumetric inspection of Hanford tank bottom plates via under-tank refractory pad air-slots.

The specific components tested for 1) functionality during active irradiation and 2) tolerance to cumulative radiation dose (until failure or upon reaching a cumulative dose test limit) were:

- four samples each of a printed circuit board (PCB) and direct current (DC) motor, which are robotic components, and
- 26 ultrasonic piezoelectric elements (samples) inside an air-slot sensor.

The robotic components are part of the RAVIS air-slot inspection crawler drive control system that is responsible for remote communication with and actuation of the air-slot inspection crawler. The failure of either of these components during under-tank deployment would require manual retrieval via the crawler's tether, which risks damage to the robot/refractory/tank. Preemptive replacement of the components at appropriately conservative dose/time intervals informed by failure dose would reduce the likelihood of under-tank failure. The components were included in radiation tolerance testing to quantify their failure doses to inform replacement intervals. The air-slot sensor is responsible for collecting ultrasonic inspection data (scan images) for the tank bottom plates during under-tank deployment. Compromised signal quality due to elevated noise levels caused by gamma radiation would compromise inspection performance. The air-slot sensor was included in radiation tolerance testing to quantify the impact of active irradiation on sensor signal quality.

The irradiation and in-situ functional tests of the PCBs, DC motors and air-slot sensor took place in June and July 2020 at the Pacific Northwest National Laboratory. Testing was performed at a gamma dose rate near 300 rad/hr., which, in the absence of under-tank dose rate data, has been conservatively estimated to be the upper-bound dose rate beneath the primary tanks at Hanford. Irradiation took place at elevated temperatures of 150-200°F to determine failure doses that reflect the compounding effects of gamma radiation and heat. The test results revealed:

- The DC motors can tolerate being actively irradiated at the high dose rate at 200°F and can tolerate a cumulative dose of 300,000 rad, that which would be incurred after 5 years of service at the 300 rad/hr dose rate. The component therefore meets minimum and preferred radiation tolerance and lifecycle requirements for robotic components.
- The air-slot sensor can tolerate being actively irradiated at the high dose rate at 150°F and can tolerate a cumulative dose of 60,000 rad, that which would be incurred after 1 year of service at the 300 rad/hr dose rate. The sensor therefore meets minimum radiation tolerance and lifecycle requirements.
- The PCB can tolerate being actively irradiated at the high dose rate, but can only tolerate a cumulative dose of 19,000 rad at 150-200°F. The PCB does not meet minimum radiation tolerance and lifecycle requirements; however, because the component is considered replaceable, it can be replaced before a cumulative dose of 19,000 rad is reached, determined through either monitoring with a dosimeter or scheduled time intervals that are calculated based on conservative estimates of under-tank dose rates.

The PCB failure dose of 19,000 rad is considered conservative since it was obtained under high radiation dose rate and temperature levels and on-board component failure dose may depend on dose rate. However, a PCB replacement schedule that is dictated by the conservative failure dose would result in low likelihoods of under-tank failure. Less conservative failure doses could be determined for different combinations of lower dose rates and temperatures, but doing so would require extensive testing and samples and the results would only be useful if they were used with under-tank dose rate measurements to calculate service hours between PCB replacement.

In the absence of under-tank dose rate data, two options for determining when to preemptively replace the PCB on an air-slot inspection crawler to mitigate the likelihood of under-tank failures are:

1. Monitor the cumulative number of hours a PCB in an inspection crawler has spent in service and replace the PCB when service time approaches 63 hours (failure time if a dose rate of 300 rad/hr is assumed) or 380 hours (failure time if a dose rate of 50 rad/hr is assumed), depending on risk tolerance. This option will likely result in the most conservative (i.e., frequent) PCB replacements.
2. Add at least one small passive dosimeter to the air-slot inspection crawler and analyze the dosimeter(s) approximately once per year to quantify cumulative dose. The PCB could then be replaced when the cumulative dose approaches a threshold set somewhere below the 19,000 rad failure dose, depending on risk tolerance. This option would reduce conservatism associated with PCB replacement frequency.

Acknowledgments

The Pacific Northwest National Laboratory would like to thank Eddyfi Technologies for providing a copy of the ICON Diagnostics software required to support testing of the PCB components, and Guidedwave for providing the multi-channel breakout box and cable adapter necessary for air-slot sensor testing.

Acronyms and Abbreviations

μ rad	micro rad (10^{-6} rad)
AEIC	air-equivalent ionization chamber
BNC	Bayonet Neill–Concelman
°C	degrees Celsius
CE	cumulative effects
cm	centimeter (10^{-2} meter)
CMS	Compact Muon Solenoid
CMOS	complementary metal-oxide semiconductor
Co-60	cobalt-60 (^{60}Co)
COM	communication
COTS	commercial off-the-shelf
DC	direct current
DMM	digital multimeter
DST	double-shell tank
°F	degrees Fahrenheit
GWPA	guided wave phased-array
Gy	gray
HEGF	High Exposure Gamma Facility
hr	hour
IC	integrated circuit
ID	identification
kGy	kiogray (10^3 gray)
kHz	kilohertz (10^3 hertz)
krad	kilorad (10^3 rad)
LiF	lithium fluoride
M&TE	measurement and test equipment
mA	milliamperere (10^{-3} ampere)
MeV	mega electron-volt (10^6 eV)
MHz	megahertz (10^6 hertz)
MIL	military
mm	millimeter (10^{-3} meter)
MOS	metal-oxide semidonductor
MOSFET	metal-oxide semiconductor field-effect transistor
Mrad	mega-rad (10^6 rad)
MS/s	mega-samples (10^6 samples) per second

mV	millivolt (10^{-3} volt)
NDE	non-destructive evaluation
PC	personal computer
PCB	printed circuit board
PHOENIX	PNNL Hanford Online Environmental Information Exchange
PNNL	Pacific Northwest National Laboratory
rad	radiation absorbed dose
RAVIS	Robotic Air-slot Volumetric Inspection System
rps	rotations per second
SEBO	single event burnout
SEE	single event effects
SEGR	single event gate rupture
SEL	single event latchup
SEU	single event upset
Si	silicon
SNR	signal-to-noise ratio
SOI	silicon-on-insulator
SOS	silicon-on-sapphire
TC	thermocouple
TID	Total Ionizing Dose
V	volts

Contents

Summary	ii
Acknowledgments.....	iv
Acronyms and Abbreviations.....	v
Contents	vii
1.0 Introduction	1
1.1 Objectives and Purpose.....	1
2.0 Background.....	3
3.0 Scope	5
3.1 RAVIS Components.....	5
3.2 Test Conditions and Duration.....	7
4.0 Description of Test Process.....	9
5.0 Test Facility, Materials, Equipment, and Setup.....	11
5.1 Test Facility, Irradiation Source, Heating Source and Dosimeters.....	11
5.1.1 Robotic Air-slot Inspection Crawler Materials, Equipment and Setup.....	15
5.2 Piezoelectric Air-slot Sensor Materials, Equipment and Setup.....	22
6.0 Test Results and Discussion	27
6.1 PCB:DC Motor Pair Test Results	27
6.2 Discussion of PCB:DC Motor Pair Test Results	31
6.3 DC Motor Test Results.....	32
6.4 Discussion of DC Motor Test Results.....	33
6.5 Air-slot Sensor Piezoelectric Element Test Results.....	33
6.6 Discussion of Air-slot Sensor Piezoelectric Element Test Results.....	35
6.6.1 Impedance Results.....	36
6.6.2 Baseline Noise Level Results	36
7.0 Summary and Conclusions.....	37
7.1 Summary	37
7.2 Conclusions	38
7.2.1 DC Motors	38
7.2.2 Air-slot Sensor.....	38
7.2.3 PCBs.....	38
Appendix I – DST Refractory Pad Temperature Data.....	I.1
Appendix II – Report of Calibration.....	II.1
Appendix III - Event Logs for Testing of RAVIS PCBs, DC Motors and Air-slot Sensor	III.1
Appendix IV - Impedance Analyzer Data for the Piezoelectric Elements of Air-slot NDE Sensor.....	IV.1
Appendix V - Radiation Damage of Electronics – Single Event Effects versus Cumulative Effects.....	V.1

Figures

Figure 1.	Clockwise from top-left: face of the air-slot sensor showing all 26 piezoelectric elements; back of air-slot sensor showing the sensor part number; DC motor; and motor controller PCB.....	6
Figure 2.	Side view of the cobalt-60 and cesium-137 irradiator in the PNNL HEGF Exposure Room, with dose rate and beam size metrics.....	11
Figure 3.	Left-Mini oven of ~0.6 ft.3 volume for testing temperatures from 72-200°F (22-93C), Right-mini oven placed in the gamma-ray field (30° port shown) of the HEGF Exposure Room for combined radiation-temperature tolerance testing.....	12
Figure 4.	HEGF Exposure Room during component placement in the mini oven located along the beam path prior to the start of irradiation.....	13
Figure 5.	HEGF Exposure Room during setup prior to the start of irradiation.....	13
Figure 6.	HEGF Control Room during equipment setup, showing the irradiator control station in the foreground and the PCB, DC motor testing station in the background.	14
Figure 7.	Screenshot of a typical HEGF irradiator control station display.	14
Figure 8.	Tested Inuktun robot components (a) motor controller PCB and (b) DC motor.	15
Figure 9.	Wiring diagram for functional testing of PCB motor driver board and a DC motor.	15
Figure 10.	Diagram of PCB and DC motor equipment configuration in the HEGF Exposure Room, and the test equipment configuration in the HEGF Control Room.....	17
Figure 11.	The PCB, DC motor testing station within the HEGF Control Room, containing the computer, power supplies, and PCB:DC motor control set.....	19
Figure 12.	The four power supplies at the PCB, DC motor testing station used to monitor the current draw and voltage associated with each PCB:DC motor pair or lone DC motor.....	19
Figure 13.	The PCB:DC motor control set at the testing station used to compare the current draw and voltage associated with the control set with the irradiated PCB: DC motor pairs.....	20
Figure 14.	The communications interfaces between the computer in the HEGF Control Room and the PCB: DC motor pairs in the HEGF Exposure Room.....	20
Figure 15.	The four PCB: DC motor pairs within the Quincy Labs mini oven, positioned at the 415 cm distance from the Co-60 irradiator in the background for irradiation at the 297 rad/hr dose rate.....	21
Figure 16.	The four powered PCB:DC motor pairs within the mini oven just prior to the start of irradiation at the 297 rad/hr dose rate.....	21
Figure 17.	The four powered lone DC motors within the mini oven just prior to the start of irradiation at the 2 krad/hr dose rate.....	22

Figure 18.	Left: Back surface of the air-slot sensor; Right: Front face of the air-slot sensor showing the round protective “wear plates” over each of the 26 piezoelectric elements in the sensor.	22
Figure 19.	Diagram of air-slot sensor test equipment configuration in the HEGF Control Room.....	23
Figure 20.	The piezoelectric air-slot sensor within the mini oven just prior to the start of irradiation at the 297 rad/hr dose rate.	24
Figure 21.	The Agilent Precision Impedance Analyzer Model 4294A, that receives waveform signals from 24 of the Sensor components and allows storage of this data on 3.5” computer disk.	25
Figure 22.	The LeCroy Model LT342 oscilloscope, and Olympus Model 5058PR High Voltage Pulser/Receiver, that is used in tandem with the oscilloscope.	25
Figure 23.	<i>Top:</i> Air-slot sensor cable connector plugged into the multichannel break-out box and interfaced with the impedance analyzer via a BNC connector on the BNC-to-Lemo adapter cable.....	26
Figure 24.	A plot of the PCB current reading (prior to spinning the motors) versus the accumulated dose.....	28
Figure 25.	The current draw for the DC motors during the motor-only test phase (2000 rad/hr for a total of 299 krad), after the associated PCBs had failed at a dose between ~19 krad and ~24.5 krad.	33
Figure 26.	<i>Top:</i> Example of an impedance vs. frequency trace for piezoelectric element E02.....	34
Figure 27.	Baseline noise level (amplitude) of the air-slot sensor piezoelectric elements before starting irradiation (unshaded) and during irradiation (shaded in light blue).....	35
Figure I.1.	Bar graph of the absolute maximum temperature and average temperature for each double-shell tank, as measured by refractory pad thermocouples.	I.1
Figure V.1.	Diagram of the two main categories of radiation effects, SEEs and long-term or CEs, and their multiple subcategories that include TID, Displacement, Transient and Catastrophic effects.	V.1
Figure V.2.	An example of the effects of relatively high radiation dose on a flash memory component.	V.2

Tables

Table 1.	Requirements for which radiation tolerance robustness testing is a verification method.....	2
Table 2.	Calculated dose expected after each tank inspection (for all 27 in-service tanks).....	3
Table 3.	M&TE for PCB and DC motor testing (hardware and software).....	18

Table 4.	M&TE for the piezoelectric elements inside the air-slot sensor (hardware).....	24
Table 5.	The Irradiation durations and dose levels at which symptoms were observed and measured for the various RAVIS components.	29
Table 6.	Estimates of doses at which negative effects of radiation will likely be observed in the most radiation-sensitive electronic components within the RAVIS system; namely, Bipolar Transistors, MOSFET Transistors, Digital ICs (Si-Bipolar, SOS/SOI, Si-MOS, Si-CMOS), and Crystal Resonators.	32
Table 7.	Calculated PCB replacement intervals in terms of service hours or quantity of tank inspections, based on the typical 19 krad dose at which PCB failure occurred during testing.....	39

1.0 Introduction

The Pacific Northwest National Laboratory (PNNL) performed radiation/temperature tolerance robustness tests for a set of printed circuit board (PCB) and direct current (DC) motor robotic components (provided by Eddyfi Technologies) and an ultrasonic guided wave phased-array (GWPA) air-slot sensor (provided by Guidedwave). The components and sensor represent those in the 2020 design of the Robotic Air-slot Volumetric Inspection System (RAVIS). This report contains the results of the high radiation dose tests performed at elevated temperatures; discusses the compounding effects of heat and radiation on component or sensor lifetime/performance; and implications for field use.

The testing was performed during the period of June 16 – July 20, 2020, within PNNL’s High Exposure Gamma Facility (HEGF) per the Test Instruction titled *NDE Technology Engineering Program for Hanford DST Non-Visual Volumetric Inspection Technology – Phase II: Radiation Tolerance Robustness Testing of RAVIS Components at Elevated Temperature*.

1.1 Objectives and Purpose

The objectives of the radiation tolerance robustness tests were to:

1. determine the cumulative gamma doses at which the operational integrity of the PCB and DC motor robotic components become compromised and fail;
2. determine whether the baseline noise level (amplitude) of an ultrasonic guided wave air-slot sensor changes as a function of cumulative gamma dose while the sensor undergoes irradiation; and
3. generate tests results that:
 - a. support decisions on the cumulative dose at which preventive maintenance (component replacement) should occur for PCBs and DC motors to significantly reduce the likelihood of under-tank failure and the need for manual retrieval;
 - b. support decisions on whether the air-slot sensor can be expected to perform well under the effects of radiation and therefore whether it is suitable for under-tank deployment and whether signal quality observed in the lab during “cold” testing represents that which can be expected during under-tank deployments; and
 - c. provide a technical basis for determining the extent to which the air-slot sensor and robotic components satisfy radiation tolerance and lifecycle requirements S-9, S-10, UT-20, and R-24 from the Phase II requirements document “Technical Requirements for Sensor and Robotic Deployment System Maturation,”¹ which are summarized in Table 1.

¹ KM. Denslow, T.L. Moran, M.R. Larche, S.W. Glass, C.P. Baker, and S.A. Bailey. 2018. NDE Technology Development Program for Non-Visual Volumetric Inspection Technology Phase II Technical Requirements for Sensor & Robotic Deployment System Maturation. PNNL-27340 Rev. 1, Pacific Northwest National Laboratory, Richland, Washington.

Table 1. Requirements for which radiation tolerance robustness testing is a verification method.

Standard Requirement #S-9	At a minimum, double-shell tank (DST) inspection technologies shall be capable of satisfying their respective functional and performance requirements for primary tank temperatures of 100°F. Preferably, DST inspection technologies would be capable of satisfying their respective requirements for primary tank sidewall and bottom plate temperatures up to 200°F.
Standard Requirement #S-10	DST inspection technologies shall be capable of satisfying their respective functional and performance requirements while receiving a radiation dose of up to 300 rad/hr.
Non-destructive evaluation (NDE) Sensor Requirement #UT-20	Sensors, cables, and co-deployed electronics shall be robust enough to satisfy their function and performance requirements for at least 1 year.
Robotic Requirement #R-24	The robotic deployment system shall be robust enough to satisfy its functions and performance requirements for at least 5 years. Exceptions are components that are considered consumable/replaceable, in which case the replacement interval of consumable/replaceable components that affect the ability to remotely control the robot shall be determined to enable preventive maintenance to avoid off-normal conditions (e.g., manual retrieval).

2.0 Background

The RAVIS is being engineered under Phase II of the *NDE Technology Engineering Program for Hanford DST Non-Visual Volumetric Inspection Technology* to prepare it for volumetric (ultrasonic) inspections of primary tank bottom plates in Hanford DST systems. Testing of the RAVIS is performed under Phase II of the Program to demonstrate the extent to which function, performance and design attribute requirements that call for requirement verification via testing are met. The purpose of requirement verification testing is to provide a technical basis for accepting the RAVIS or requiring additional improvements and deciding its suitability for qualification and deployment in a DST system. The full scope of functional, performance and robustness testing established for Phase II is defined in the Phase II Test Plan.

The tolerance of RAVIS sub-systems or sub-system components to gamma radiation is a design attribute requirement (Standard Requirement S-10) that was imposed to assure:

1. RAVIS robotic components would be designed to perform their functions at the expected performance levels under the effects of radiation and endure at least five years of periodic use in the tank farms, and
2. the RAVIS air-slot sensor would be designed to perform its functions at the expected performance levels under the effects of radiation and endure at least one year of periodic use in the tank farms.

Testing the effects of radiation on sub-systems or components to evaluate the impact of radiation on their functions/performances and lifecycle is a type of “robustness test.”

The nominal and upper-bound gamma dose rates that have been estimated for a primary tank are 50 rad/hr and 300 rad/hr, respectively. The estimated number of hours of RAVIS exposure per year is 200 hours, or those needed to complete approximately 2.5 tank inspections. Table 2 shows the cumulative dose in kilorad (krad) expected after each year of service for the estimated nominal and upper-bound dose rates.

Table 2. Calculated dose expected after each tank inspection (for all 27 in-service tanks).

Cumulative #years	1	2	3	4	5	6	7	8	9	10	10.7
Cumulative #hrs	200	400	600	800	1000	1200	1400	1600	1800	2000	2140
Cumulative #tanks inspected	2.5	5	7.5	10	12.5	15	17.5	20	22.5	25	27
Cumulative dose at 50 rad/hr dose rate	10 krad	20 krad	30 krad	40 krad	50 krad	60 krad	70 krad	80 krad	90 krad	100 krad	107 krad
Cumulative dose at 300 rad/hr dose rate	60 krad	120 krad	180 krad	240 krad	300 krad	360 krad	420 krad	480 krad	540 krad	600 krad	642 krad

The nominal and upper-bound dose rates of 50 rad/hr and 300 rad/hr, respectively, are considered to have high uncertainties because they are based on estimates made by tank farm subject matter experts. Furthermore, dose rates from tank to tank may be very different.

Therefore, the dose rates and the calculated cumulative doses reached in year in Table 2 are subject to change if quantitative measurements of dose rate are made available in the future and found to be significantly different (e.g., lower) than the estimated 50-300 rad/hr dose rates. For this reason, the matrix in Table 2 was used only to guide the selection of 1) the cumulative dose intervals at which sub-system/component functional tests/measurements were performed, and 2) cumulative dose limit for the radiation tolerance robustness tests. Observations and measurements of sub-system/component functions made at a sampling of dose intervals allowed failure doses (cumulative dose at which component failure occurs) to be experimentally determined with relatively high resolution. The failure dose data can be used later to re-calculate expected component lifetimes and replacement intervals, if under-tank dose rate measurements become available, without having to rerun the radiation tolerance robustness tests.

In 2018, the set of calculated cumulative doses from Table 2 was sampled and used in a scoping test that was performed with one PCB and one DC motor to coarsely estimate the lifecycles of the two components (i.e., dose at which failure occurred). The scoping test was performed at the Washington State University Nuclear Science Center in Pullman, WA and entailed exposing the components to gamma radiation from a cobalt-60 source. Irradiation was performed at a test dose rate of 500 rad/hr and functional testing was performed at pre-set time intervals that corresponded with pre-selected cumulative dose intervals of 12 krad, 24 krad, 48 krad and 72 krad. Irradiation was halted at each dose intervals to test PCB and DC motor functionality ex-situ and then returned to the radiation exposure room. The PCB sample was found to have failed between dose intervals 48 krad and 72 krad while the DC motor had not failed by the time the test was terminated at 72 krad.

Three different sets of dry couplant membranes, which may be vulnerable to the effects of radiation and will be installed on the RAVIS's ultrasonic guided wave air-slot sensor, were exposed to gamma radiation during the same 2018 scoping test. The dry couplant membranes only need to tolerate a dose accumulated during one day of real tank inspection operations since the membranes will be replaced daily. Therefore, the membranes were exposed to target doses of 500 rad (10-hr shift at 50 rad/hr) to 3,000 rad (10-hr shift at 300 rad/hr) during the scoping test. The average signal-to-noise ratio of ultrasonic energy reflected from flaws in a test plate associated with an air-slot sensor coupled with unexposed dry couplant membranes and then the exposed/irradiated dry couplant membranes showed there was little perceivable impact on signal-to-noise ratio between the samples and therefore no perceivable damage to the membranes.¹

The results of the 2018 scoping test were intended to identify the narrower cumulative dose ranges over which functional testing should occur, and in finer dose intervals, in follow-on radiation tolerance robustness tests to generate higher-resolution lifecycles/failure times. The testing reported here represent the follow-on testing.

¹ K.M. Denslow, T.L. Moran, M.R. Larche, S.W. Glass, K.D. Boomer, T.A. Wooley, J.R. Gunter, J.P. Rice, S.E. Kelly, D.M. Stewart, C. Borigo, R. Love, A. Reese, G. Hamilton, C. Mo, M. Osman, A. Porter, E. Loeffler, F. Chavarria, and D. Garcia, "Progress on Advancing Robotic Ultrasonic Volumetric Inspection Technology for Hanford Under-tank Inspection -19474," Waste Management Symposia 2019, March 3-7, 2019, Phoenix, Arizona (2019).

3.0 Scope

The 2020 tests were performed at finer dose intervals than the 2018 scoping tests to obtain higher-resolution PCB and DC motor failure times. The tests were also performed using a larger sample set of PCBs and DC motors; were performed continuously by testing PCB and DC motor functionality as irradiation was occurring; and were performed at controlled/elevated temperatures to determine the impact that compounding effects of heat and radiation have on failure dose. The tests were leveraged to determine the effects of active radiation on air-slot sensor signal noise level (amplitude). Dry couplant membranes associated with the air-slot sensor were not re-tested because three dry couplant membrane samples were exposed for each accumulated dose during the 2018 scoping test, which was satisfactory. The effects of high temperatures on the membranes must be and were evaluated using a test setup that includes a mock-up tank plate such as that located in the Applied Process Engineering Laboratory.

The remainder of this section describes the types of components included in testing, the quantity of each, and the conditions under which testing occurred.

3.1 RAVIS Components

To manage the scope and cost of radiation tolerance robustness testing, the test was reserved for RAVIS sub-systems or components that meet one or more of the following criteria:

1. have known vulnerability to radiation-induced degradation and/or temperature-induced degradation;
2. would have a high cost/safety consequence if failure due to radiation damage occurred during an under-tank deployment (i.e., its failure during an under-tank deployment in a refractory pad air-slot would result in an off-normal condition and lead to manual retrieval via the RAVIS tether that could damage the robot, the sensor and the refractory pad/tank);
3. would have a high cost consequence if unforeseen poor performance due to the effects of radiation was realized/observed for the first time during a real tank inspection (e.g., substandard positioning or measurement performance that would yield substandard inspection results, and be of little value to the DST integrity management program);

and either

1. do not have known radiation tolerances because they have not been tested previously or have not been published in publicly available literature, or
2. have large radiation tolerance uncertainties due to small sample sizes, are electronics tested under significantly higher test dose rates, or have a low degree of similarity between published components/sub-systems and RAVIS components/sub-systems.

The RAVIS sub-systems and components that were included in the scope of radiation tolerance robustness testing that meet the above-listed criteria are:

1. the PCB and DC motor component inside the air-slot inspection crawler, and
2. the ultrasonic Guided Wave Phased-Array (GWPA) sensor (air-slot sensor).

A photo of the components is provided in Figure 1. The following quantities of each component/sub-system were included in radiation tolerance robustness testing:

- Quantity one (1) ultrasonic GWPA air-slot sensor sub-system engineered by Guidedwave in 2018. The sensor (*Hanford-Probe A*) contains 26 ultrasonic piezoelectric elements, each representing one sample, that are surrounded/cast in place with sound damping material and enclosed in a stainless steel housing.

The 2018 *Hanford-Probe A* sensor will not be deployed for tank bottom inspections due to its low signal fidelity, but its design, piezoelectric elements, other materials, and construction are highly representative of those used in the engineering of newer air-slot sensors that will be deployed for tank bottom inspections.

- Quantity four (4) PCB samples of the same model (custom PCB by Inuktun/Eddyfi).
- Quantity four (4) DC motors of the same model (Maxon brand, 2.5W, 12V, 131:1 ratio).

The PCB and DC motor components are associated with the drive control system of the air-slot inspection crawler (“baby-bot”) aspect of the marsupial deployment/inspection robotic system that has been engineered by Inuktun/Eddyfi Technologies. A larger quantity of PCB and DC motor samples to represent a statistically representative sample set (e.g., at least 10 each) were not purchased for testing due to the cost of the components.

Note: A fifth PCB sample and a fifth DC motor sample were not irradiated and used as “control” samples.

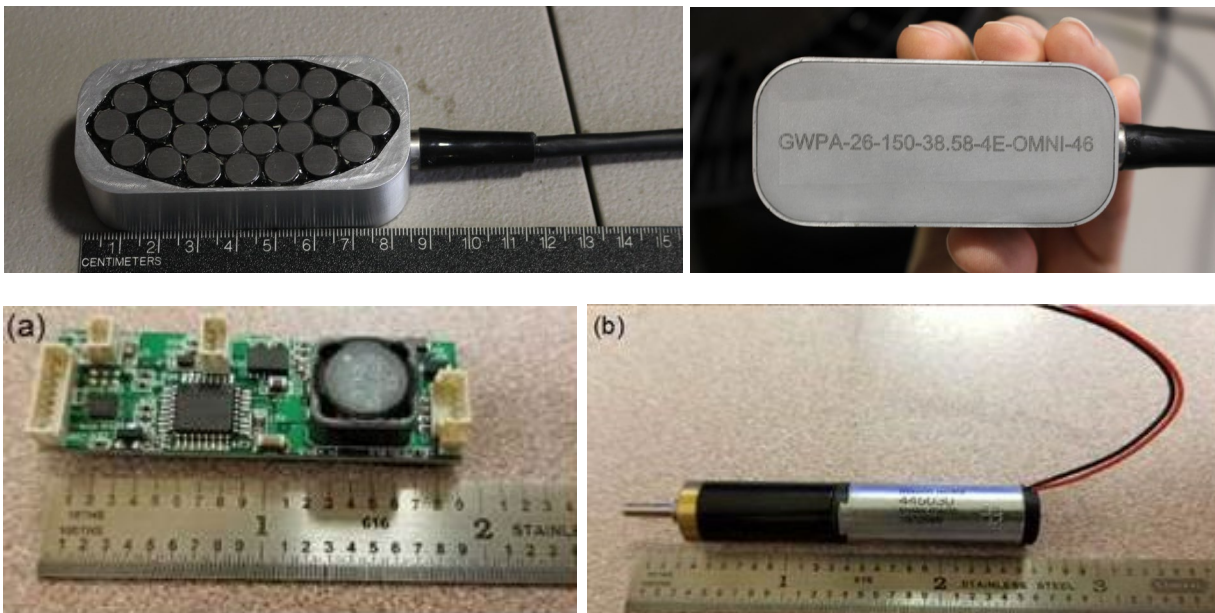


Figure 1. Clockwise from top-left: face of the air-slot sensor showing all 26 piezoelectric elements; back of air-slot sensor showing the sensor part number; DC motor; and motor controller PCB.

3.2 Test Conditions and Duration

Radiation tolerance robustness testing was performed under a limited set of test conditions that represent conservative (high) radiation levels and temperatures expected under Hanford primary tanks.

The following test conditions were selected for radiation tolerance robustness testing:

Dose rate and Duration - Radiation tolerance testing of PCBs, DC motors and the air-slot sensor was performed at a gamma dose rate of 297 rad/hr, which is nearly equivalent to the conservatively high dose rate of 300 rad/hr. estimated for a Hanford DST environment. The 297 rad/hr test dose rate is absorbed dose relative to air, known as Air Kerma. The reason for using a testing dose rate near the conservative tank farm dose rate instead of accelerating testing by using a higher dose rate is the failure times of electronic components like those found in the PCBs can depend on the dose rate to which they are exposed.

Testing at the 297 rad/hr dose rate was performed for the four PCBs and the four DC motors until PCB failure occurred, at which point the PCBs were removed and testing proceeded with the four DC motors alone at an elevated dose rate of 2 krad/hr. The elevated dose rate was used to accelerate testing to reach the ~300 krad point, which was the test limit established for the robotic components because it represents the maximum dose expected after five years of service at the upper-bound dose rate of 300 rad/hr. It is the minimum life expectancy requirement placed on the RAVIS robotic sub-system. Testing at the elevated 2 krad/hr dose rate with the DC motors to determine if they failed before 300 krad was acceptable because, based on motor component type/materials, the DC motor failure dose would not be sensitive to dose rate.

Testing at the 297 rad/hr dose rate was performed for the air-slot sensor until 67 krad was reached, which was near the 60 krad test limit established for the air-slot sensor because it represents one year of service at the upper-bound dose rate of 300 rad/hr – the minimum life expectancy requirement placed on the sensor. The reasons for using a testing dose rate near the conservative tank farm dose rate instead of accelerating testing with a higher dose rate were:

1. it was not necessary to observe piezoelectric element baseline noise amplitudes at a dose rate higher than the conservative upper-bound dose rate, and
2. it was desirable to observe piezoelectric element baseline noise amplitudes over a time period representative of that expected during an under-tank inspection campaign (~10 days) to determine if any trends in noise level as a function of cumulative dose would occur.

Temperature - The PCBs and DC motors were exposed to a maximum temperature of 200°F during irradiation to capture compounding effects of heat and radiation that may accelerate failure. Although the maximum average tank temperature is currently near 165°F (AZ-101) and a majority of tanks have an average temperature below 100°F, as shown in Appendix I, a test temperature of 200°F was selected to serve as a conservative upper-bound temperature for the following:

1. maximum current tank operating temperatures,
2. heat generated by the RAVIS air-slot inspection crawler during deployment, or
3. future tank operating temperatures if allowed to increase (by decreasing ventilation).

The air-slot sensor *Hanford-Probe A* (2018 prototype) was exposed to a maximum temperature of 150°F during irradiation. The reason for the lower test temperature is the materials of construction used in *Hanford-Probe A* represent those of the air-slot sensor(s) intended for under-tank deployment, which have not yet been adapted to tolerate higher temperatures. The air-slot sensor(s) intended for under-tank deployment (2019 *Hanford-Probe A* and/or 2020 *Hanford-Probe A*) will only be used to inspect tanks with bottom temperatures under 150°F (and with “V-shaped” air-slot cross-sections).

4.0 Description of Test Process

This section contains descriptions of the test intervals, test methods and test criteria for the PCBs, DC motors, and the piezoelectric elements inside the air-slot sensor. Descriptions of test equipment and test setups for each type of component are included. Additional details are provided in the Test Instruction *NDE Technology Engineering Program for Hanford DST Non-Visual Volumetric Inspection Technology – Phase II: Radiation Tolerance Robustness Testing of RAVIS Components at Elevated Temperature*.

PCB Test Intervals, Test Methods and Test Criteria: Functional tests of the PCBs were performed during their irradiation at coarse dose intervals of approximately 2-4 krad until 16.5 krad was achieved, at which point functional tests were performed more frequently at finer dose intervals of approximately 1 krad (equivalent to approximately 3 hrs of exposure at the 297 rad/hr dose rate) until all four PCB samples had failed (3-4 days). Data collection was performed 12 separate times over the irradiation period.

The functional tests of the PCBs during irradiation entailed using diagnostic software developed for the PCBs to command a PCB to spin a connected DC motor forward and backward. The current draw reading displayed on the DC power supply coupled to a PCB:DC motor pair and the communication feedback provided in the diagnostic software were used to determine whether damage had occurred to a PCB. If communications with the PCB via the software were successful (i.e., no errors displayed) and the power supply current draw was ≥ 0 amps, then the PCB (and DC motor) were deemed functional and unaffected by active irradiation. If the PCB was unresponsive, communication errors were observed in the software, and no current draw was observed on the power supplies then several troubleshooting steps were performed per the Test Instruction to isolate the failure to the PCB, DC motor, software or wiring harness. When the PCB was deemed the failed component, it was removed from the exposure room for further diagnostic testing to identify the on-board component(s) responsible for PCB failure.

DC Motor Test Intervals, Test Methods and Test Criteria: Upon failure of all four PCBs and their subsequent removal from the exposure room, the testing dose rate was increased to accelerate testing for the DC motors alone for six additional days. Functional tests of the DC motors were performed during their irradiation at coarse dose intervals of approximately 21 krad (equivalent to 70 hrs of exposure at the upper-bound 300 rad/hr dose rate, or roughly one tank inspection). Data collection was performed 14 separate times over the irradiation period.

The functional tests of the DC motors during irradiation entailed using only a power supply to spin each DC motor. The current draw readings displayed on the power supply connected to each DC motor were used to determine whether damage had occurred to a DC motor. If the power supply current draw was ≥ 0 amps, then the DC motor was deemed functional.

Air-slot Sensor Test Intervals, Test Methods and Test Criteria: The piezoelectric elements in the air-slot sensor were characterized during their irradiation nearly every day over the 10-day irradiation period until a cumulative dose of 67 krad was reached. Data collection with the impedance analyzer and the oscilloscope were performed nine separate times over the irradiation period.

Two parameters were measured during sensor irradiation: the electrical impedance of the sensor's piezoelectric elements and the baseline noise amplitude of the elements. The electrical impedance of each piezoelectric element was measured over a frequency range of 100 kHz to 300 kHz – to capture the data for the 150 kHz resonance mode of the piezoelectric elements –

using an impedance analyzer. The nominal baseline noise amplitude of an element was measured by using an ultrasonic pulser/receiver unit to pulse/excite the element with a standard 400-volt, 10 nanosecond broadband electric “spike” pulse, receive and condition the resulting signals from the element, average a set of 500 signals that were 5-milliseconds in duration, and analyze the nominal baseline noise amplitude of the average signal.

The noise amplitude data was quantified during irradiation using the oscilloscope’s on-board computer, screen and measurement cursors. A relative change in noise amplitude (voltage) of less than $\pm 10\%$ (well within error) while under irradiation indicated the element was stable and unaffected by gamma radiation at the 300 rad/hr dose rate. The impedance data was saved during testing and analyzed after irradiation had concluded. A relative change in impedance of less than $\pm 10\%$ (well within error) while under irradiation would indicate the element was stable and unaffected by gamma radiation.

5.0 Test Facility, Materials, Equipment, and Setup

5.1 Test Facility, Irradiation Source, Heating Source and Dosimeters

The gamma-ray irradiator used for radiation tolerance robustness tests is the cobalt-60 and cesium-137 irradiator in the PNNL HEGF, located inside Building 318 in the 300 Area. The custom irradiator contains an underground carousel with six ports that accommodate six cesium-137 and cobalt-60 sources that vary from low to ultra-high activity levels, resulting in a continuum of dose rates from approximately 30 micro-rad per hour (30 μ rad/hr) to over 5 mega-rad per hour (5 Mrad/hr). A photo of the irradiator is provided in Figure 2.

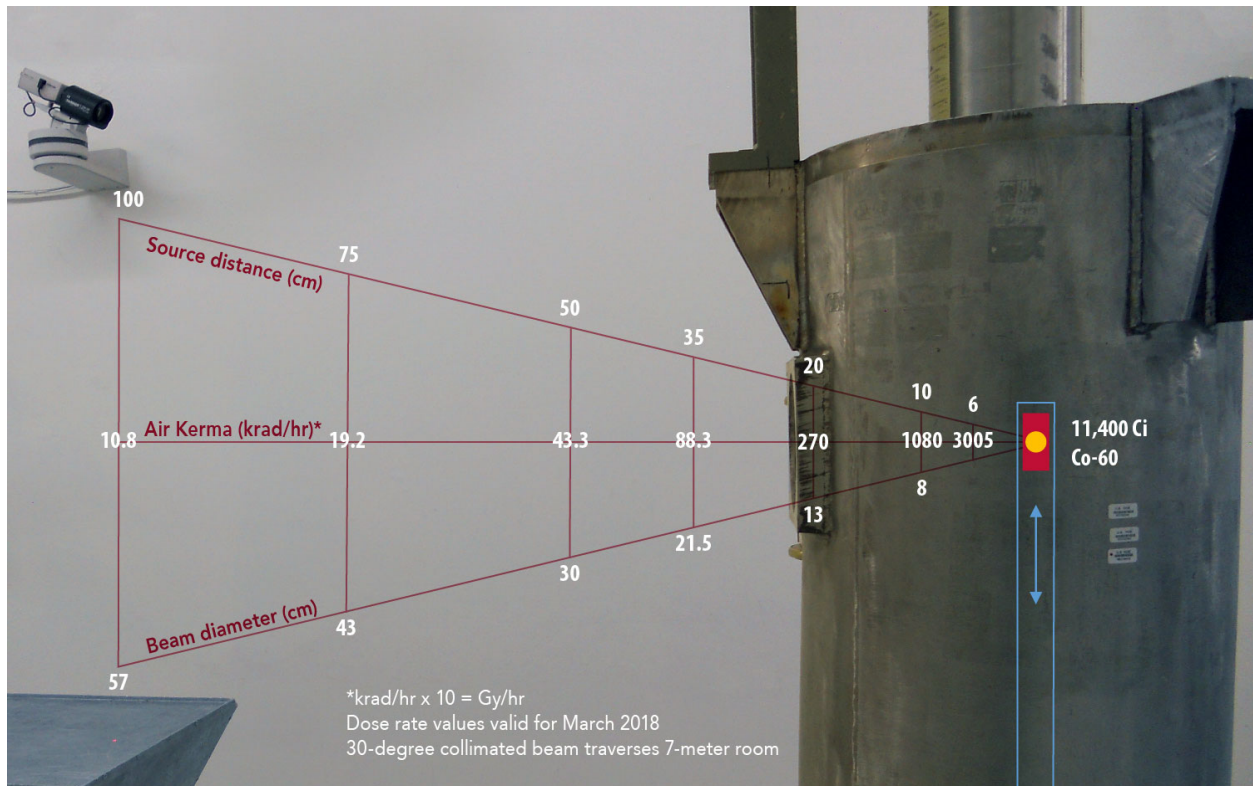


Figure 2. Side view of the cobalt-60 and cesium-137 irradiator in the PNNL HEGF Exposure Room, with dose rate and beam size metrics. The subject test location will be at a source distance of approximately 4 meters.

A cobalt-60 gamma radiation source was used for radiation tolerance robustness testing of the PCBs, DC motors and air-slot sensor. The reasons for selecting a cobalt-60 source over a cesium-137 source were:

1. a cobalt-60 source provides a spectrum that has an average energy somewhat higher than cesium-137, which will conservatively represent the spectrum that would be expected in a DST environment from the gamma-emitting cesium-137 (0.66 MeV max) and beta-emitting strontium-90 (2.3 MeV max for Yttrium-90) that would produce bremsstrahlung in the steel walls of with energies above cesium-137;
2. given the RAVIS components have a thickness to them, and during real deployment will be shielded/shadowed by other structures on the robotics package, using a radiation field with

a higher average energy than cesium-137 provided a somewhat conservative dose to the components and thus supported a conservative test; and

3. the cobalt-60 beam at a dose rate of 300 rad/hr is many feet in diameter and therefore allowed the four PCBs, four DC motors, the air-slot sensor and the mini oven that contained them to fit within the beam.

A forced air mini oven (0.6 cubic foot, 800W, 115V) shown in Figure 3 was used to house and control the temperature of the PCBs, DC motors and air-slot sensor during irradiation by the cobalt-60 source in the HEGF Exposure Room. The mini oven's temperature range is approximately 30-200 Celsius and is controlled to within approximately ± 2 C of the target temperature.



Figure 3. Left-Mini oven of ~0.6 ft.3 volume for testing temperatures from 72-200°F (22-93C), Right-mini oven placed in the gamma-ray field (30° port shown) of the HEGF Exposure Room for combined radiation-temperature tolerance testing.

The exact dose rate within the oven (where test components were placed) was measured prior to the start of irradiation using a small volume, reference-class ionization chamber with rad/hr and Gy/hr calibration coefficients traceable to the National Institute of Standards and Technology.

The number of minutes the cobalt-60 source was exposed and irradiating the test components was monitored using the automated timer on the irradiation control station panel in the radiation-free HEGF Control Room. The timer display was always available and used to record the times at which in-situ functional tests of the components under irradiation were performed. The recorded timer values were later used to calculate the exact total integrated dose experienced by the test components at each test interval and at the conclusion of irradiation. To verify the dose received by the test components, passive dosimetry (LiF or radiachromic dosimeter films) were placed on the front and back of the mini oven during irradiations and later analyzed for total integrated dose. Calibration information for the dosimetry equipment, oven, and thermocouples is provided in Appendix II.

Photographs of the HEGF Exposure Room and Control Room are provided in Figure 4 through Figure 7.



Figure 4. HEGF Exposure Room during component placement in the mini oven located along the beam path prior to the start of irradiation.



Figure 5. HEGF Exposure Room during setup prior to the start of irradiation. Foreground: gamma-ray irradiator; Background: mini oven on a pedestal positioned along the beam path.

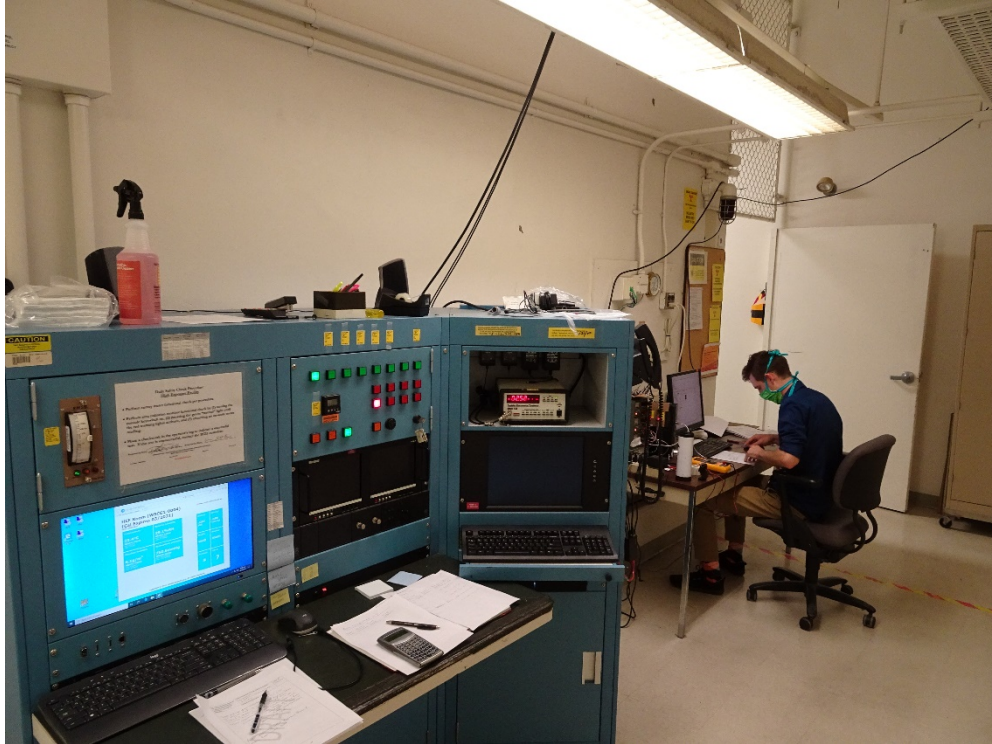


Figure 6. HEGF Control Room during equipment setup, showing the irradiator control station in the foreground and the PCB, DC motor testing station in the background.

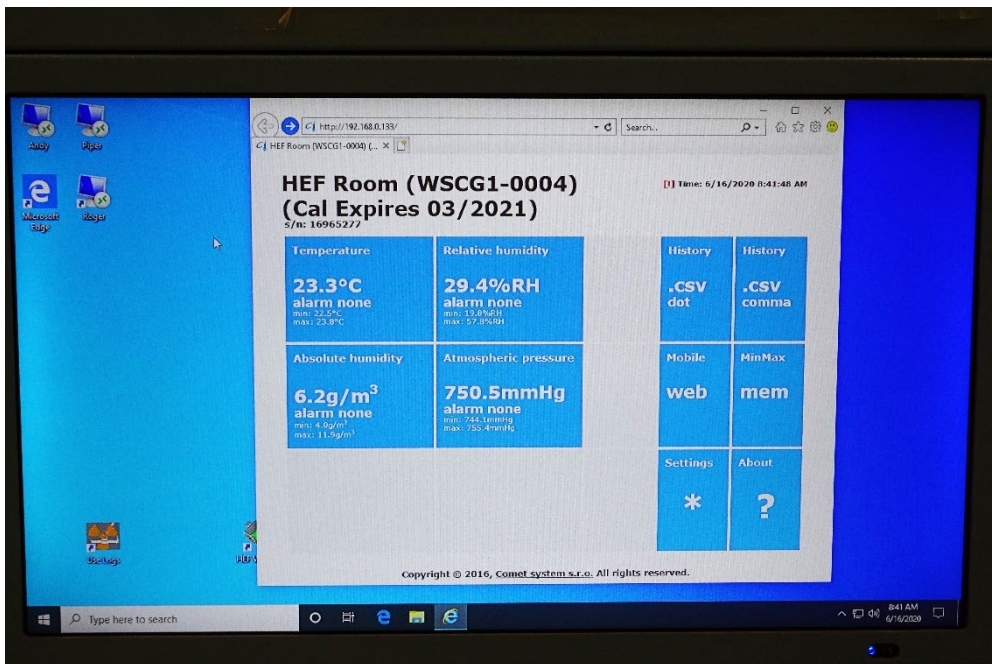


Figure 7. Screenshot of a typical HEGF irradiator control station display.

5.1.1 Robotic Air-slot Inspection Crawler Materials, Equipment and Setup

The RAVIS robotic components evaluated for radiation tolerance were four custom PCBs designed by Inuktun/Eddyfi Technologies and four Maxon DC motors. These components are pictured in Figure 8.

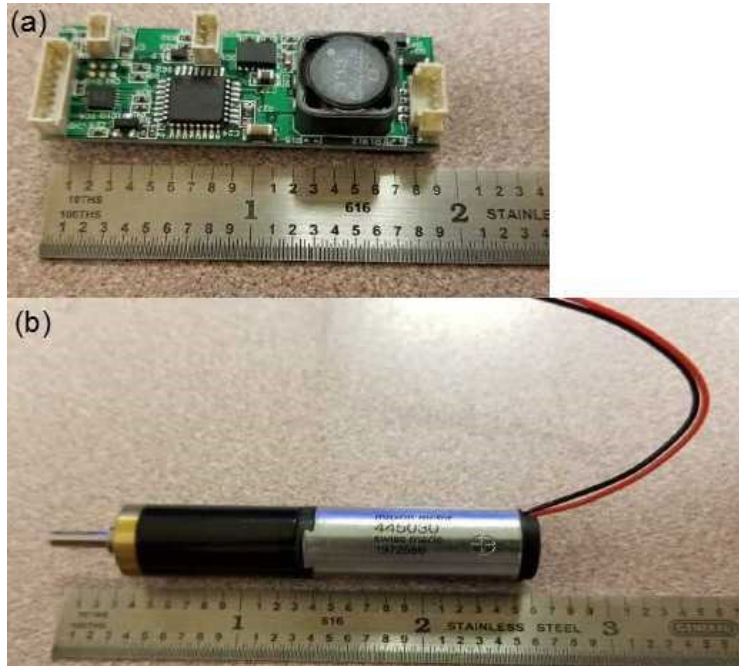


Figure 8. Tested Inuktun robot components (a) motor controller PCB and (b) DC motor.

The PCB controls the DC motor in the RAVIS air-slot inspection crawler. During radiation tolerance robustness testing, each of the five PCBs was paired with a DC motor and connected with wire harnesses (provided with the PCBs and DC motors) to mimic the connections within the RAVIS air-slot inspection crawler. Inuktun/Eddyfi ICON Diagnostics software that had been loaded onto a computer was used to interface with each PCB and control each PCB:DC motor pair via a USB/RS-485 dongle. The connections are illustrated in the wiring diagram in Figure 9.

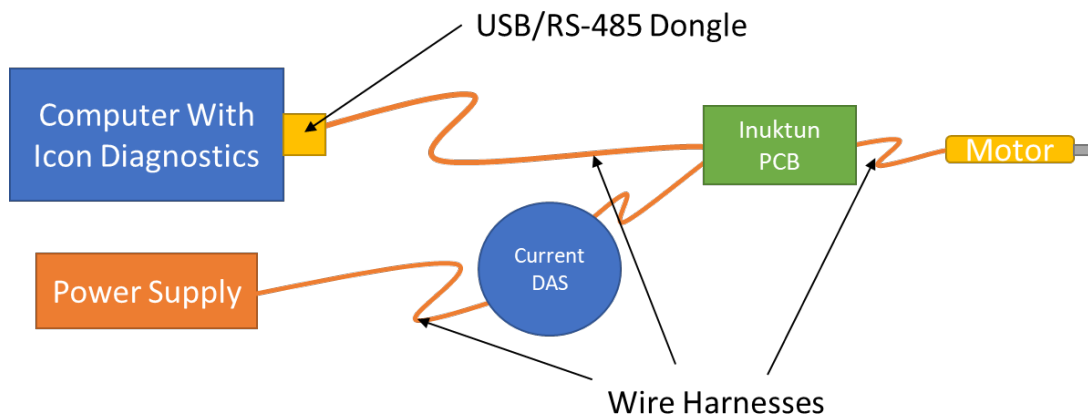


Figure 9. Wiring diagram for functional testing of PCB motor driver board and a DC motor.

The four sets of paired PCBs and DC motors connected with wire and data harnesses per Figure 9 were placed in the mini oven inside the HEGF Exposure Room while the fifth PCB:DC motor pair (control set) and all other test equipment for PCB:DC motor pair tests were placed in the radiation-free HEGF Control Room. The schematic in Figure 10 shows the general configuration of the PCBs, DC motors, and test equipment in the HEGF Control Room and HEGF Exposure Room.

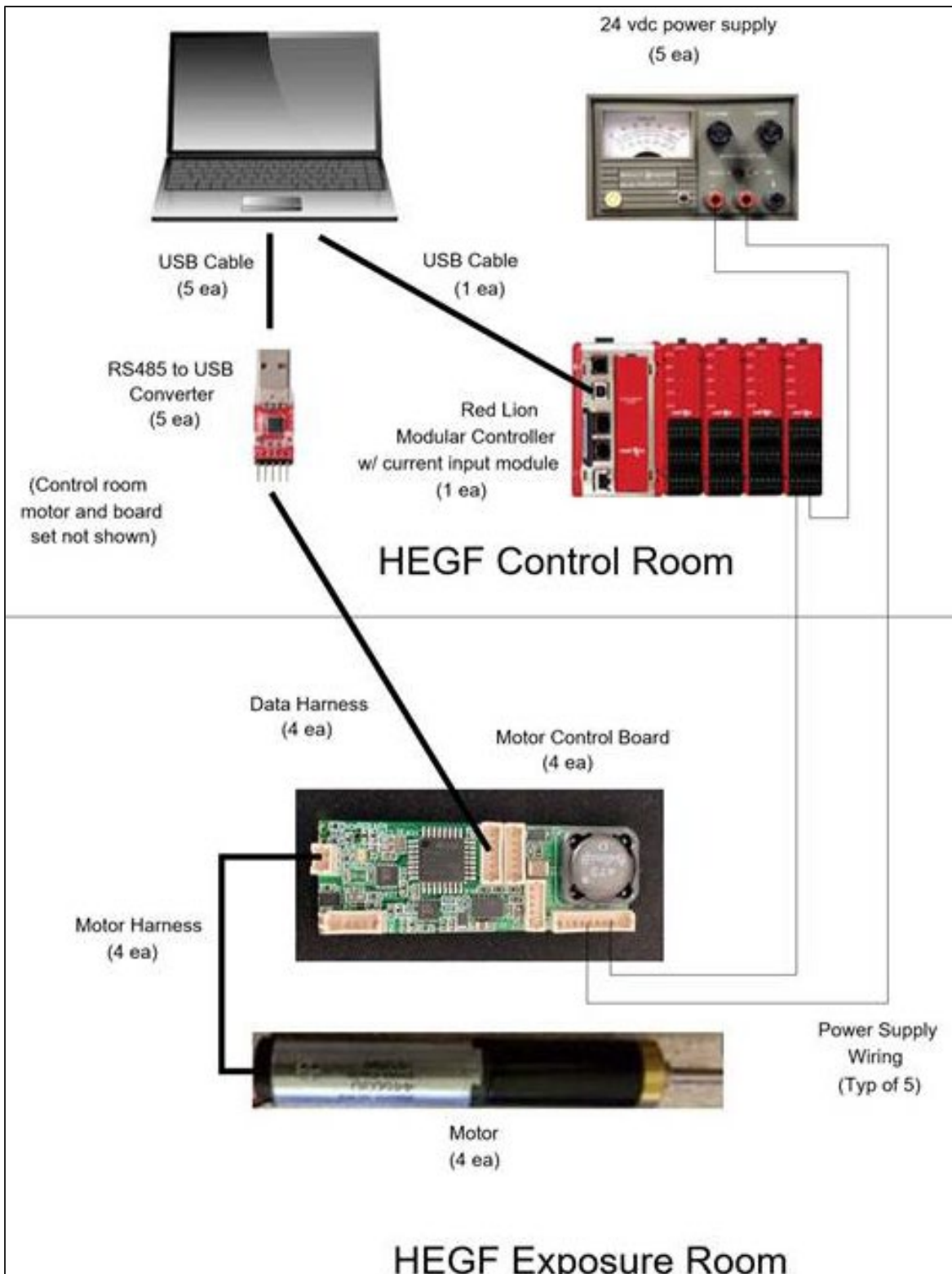


Figure 10. Diagram of PCB and DC motor equipment configuration in the HEGF Exposure Room, and the test equipment configuration in the HEGF Control Room.

The measurement and test equipment (M&TE) utilized for the paired PCB:DC radiation tolerance robustness tests are listed in Table 3 (hardware and software). Photographs of equipment setups in the HEGF Exposure Room and Control Room are provided in Figure 11 through Figure 17.

Table 3. M&TE for PCB and DC motor testing (hardware and software).

Equipment	I.D.#	Calibration Exp. Date	Application/Notes
PCB	Inuktun/Eddyfi Part number VT50/3066729-F02	N/A	Component under test board, custom Inuktun/Eddyfi component of air-slot inspection crawler
2.5W, 12V, 131:1 ratio DC motor	Inuktun/Eddyfi Part number 3069851-A	N/A	Component under test, Maxon-brand component of air-slot inspection crawler
Co-60 field within Oven	318-545	6/14/2021	Calibrated just prior to RAVIS testing
Quincy Labs Mini Oven	Model 10AF s/n A1-2674	See Thermocouples	RAVIS components were within this Oven, which was within the Co-60 field
Oven TC/Module system	40007, 4009, 40011	6/14/2021	Oven thermocouples and associated readout module
Data Logger for Oven temperatures	Model VC-TC s/n 103CC00180	6/14/2021	Data Logging Oven temperatures
HEGF temperature/pressure	WSCG1-0004	03/2021	Ambient conditions used to correct signal from ionization chamber
HEGF Timer	SWRC1-0002	03/2021	Provides minutes that Co-60 source is exposed
Fluke 77IV Digital Multimeter (DMM)	MMFLC-0005	05/19/2021	For confirming/measuring power supply voltages
24 VDC Power Supply	HP 6234A s/n 1822A-00186	N/A	Not M&TE. Voltage set using DMM. Two channel power supply that powered systems 1 and 2
24 VDC Power Supply	HP 6218A s/n 2008A-09772	N/A	Not M&TE. Voltage set using DMM. One channel power supply that powered system 3
24 VDC Power Supply	HP 6218A s/n 2008A-09771	N/A	Not M&TE. Voltage set using DMM. One channel power supply that powered system 4
24 VDC Power Supply	Triad WDU24-500 s/n none	N/A	Not M&TE. Voltage confirmed using DMM. One channel power supply that powered system 5 / control
Inuktun ICON Diagnostics	N/A	N/A	ICON Diagnostics software is a freeware provided by Eddyfi Technologies



Figure 11. The PCB, DC motor testing station within the HEGF Control Room, containing the computer, power supplies, and PCB:DC motor control set.

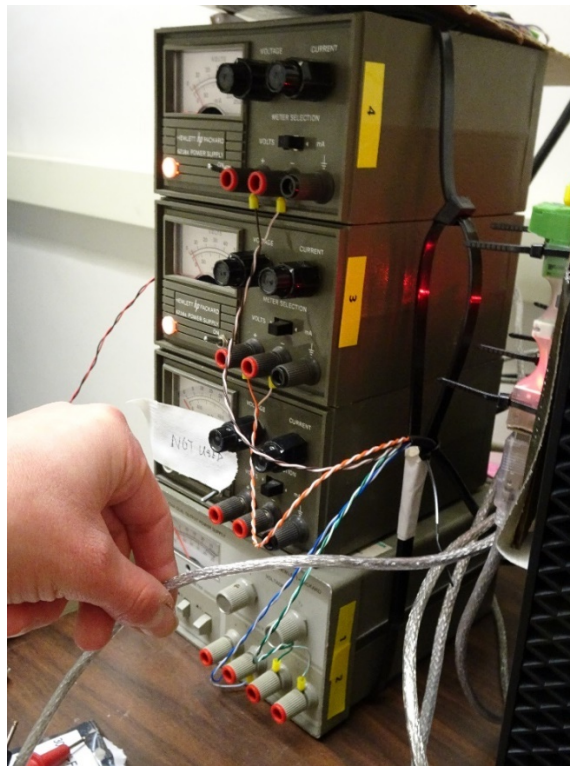


Figure 12. The four power supplies at the PCB, DC motor testing station used to monitor the current draw and voltage associated with each PCB:DC motor pair or lone DC motor.

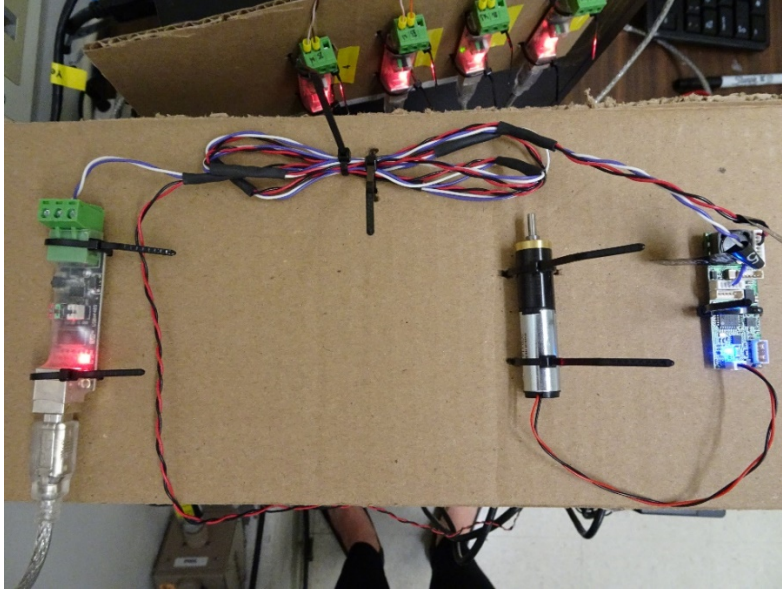


Figure 13. The PCB:DC motor control set at the testing station used to compare the current draw and voltage associated with the control set with the irradiated PCB: DC motor pairs. *Left*: communications interface for the PCB:DC motor control set; *Middle*: DC motor control sample; *Right*: PCB control sample.



Figure 14. The communications interfaces between the computer in the HEGF Control Room and the PCB: DC motor pairs in the HEGF Exposure Room.

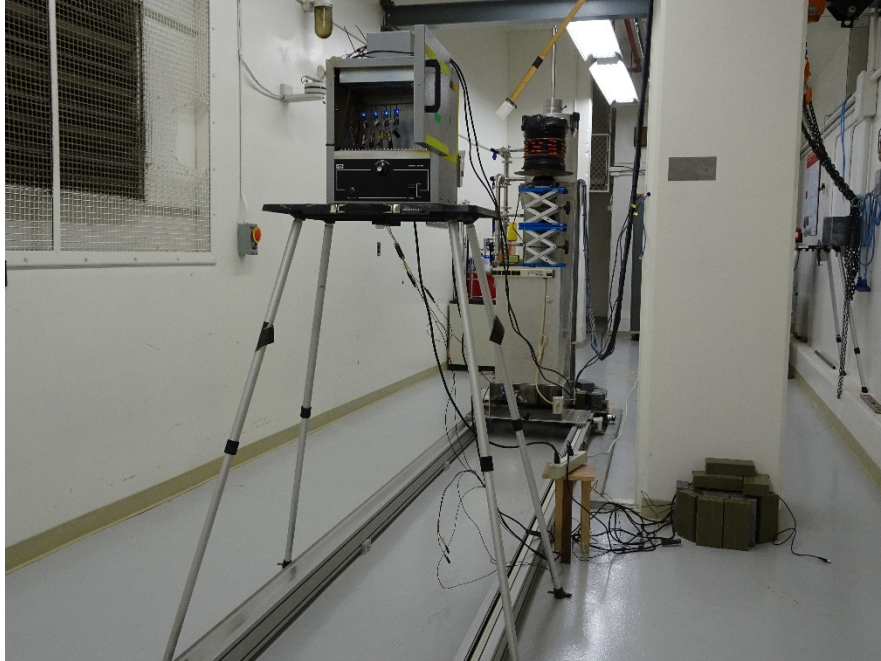


Figure 15. The four PCB:DC motor pairs within the Quincy Labs mini oven, positioned at the 415 cm distance from the Co-60 irradiator in the background for irradiation at the 297 rad/hr dose rate.

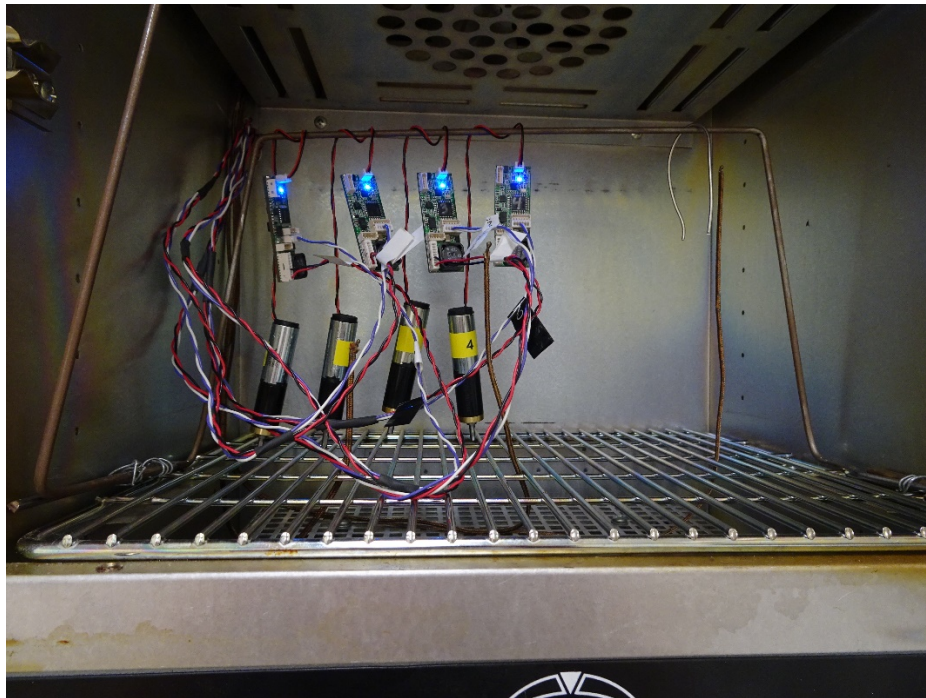


Figure 16. The four powered PCB:DC motor pairs within the mini oven just prior to the start of irradiation at the 297 rad/hr dose rate.



Figure 17. The four powered lone DC motors within the mini oven just prior to the start of irradiation at the 2 krad/hr dose rate.

5.2 Piezoelectric Air-slot Sensor Materials, Equipment and Setup

The air-slot sensor evaluated for radiation tolerance was a custom piezoelectric ultrasonic GWPA sensor designed by Guidedwave and manufactured by Olympus Scientific Solutions. As stated previously, the sensor is the 2018 prototype air-slot sensor (Hanford-Probe A) and will not be deployed for tank bottom inspections, but its design, materials and construction are highly representative of those that were used in the air-slot sensors that are intended for tank bottom inspections. Photographs of the air-slot sensor used for radiation tolerance robustness testing are provided in Figure 18.

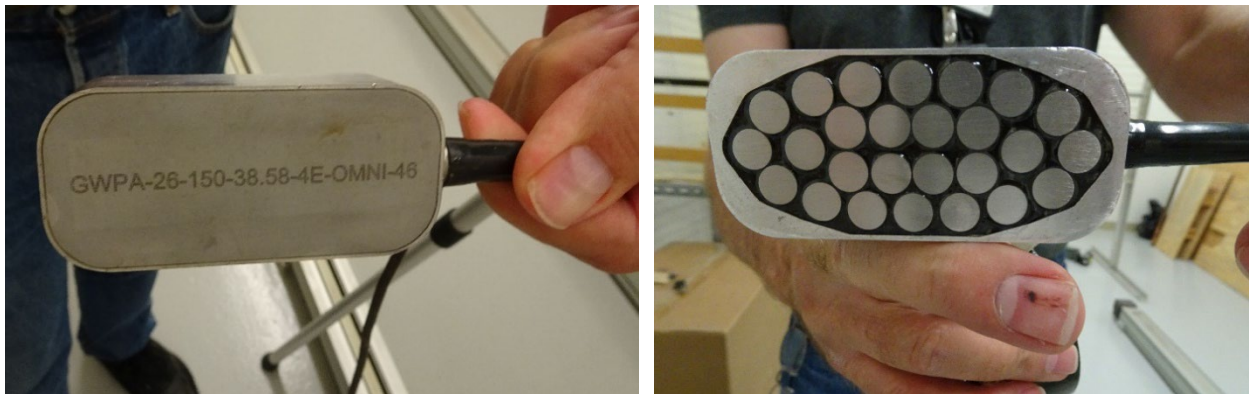


Figure 18. Left: Back surface of the air-slot sensor; Right: Front face of the air-slot sensor showing the round protective “wear plates” over each of the 26 piezoelectric elements in the sensor.

The air-slot sensor was placed in the HEGF Exposure Room mini oven and its 150-ft. long cable was routed from the mini oven to the radiation-free HEGF Control Room where the end connector was interfaced with the impedance analyzer or ultrasonic pulser/receiver and oscilloscope. A multichannel break-out box with BNC-to-Lemo adapter cable was used to interface the connector with the test equipment. The schematic in Figure 19 shows the general configuration of the air-slot sensor and test equipment in the HEGF Control Room and HEGF Exposure Room.

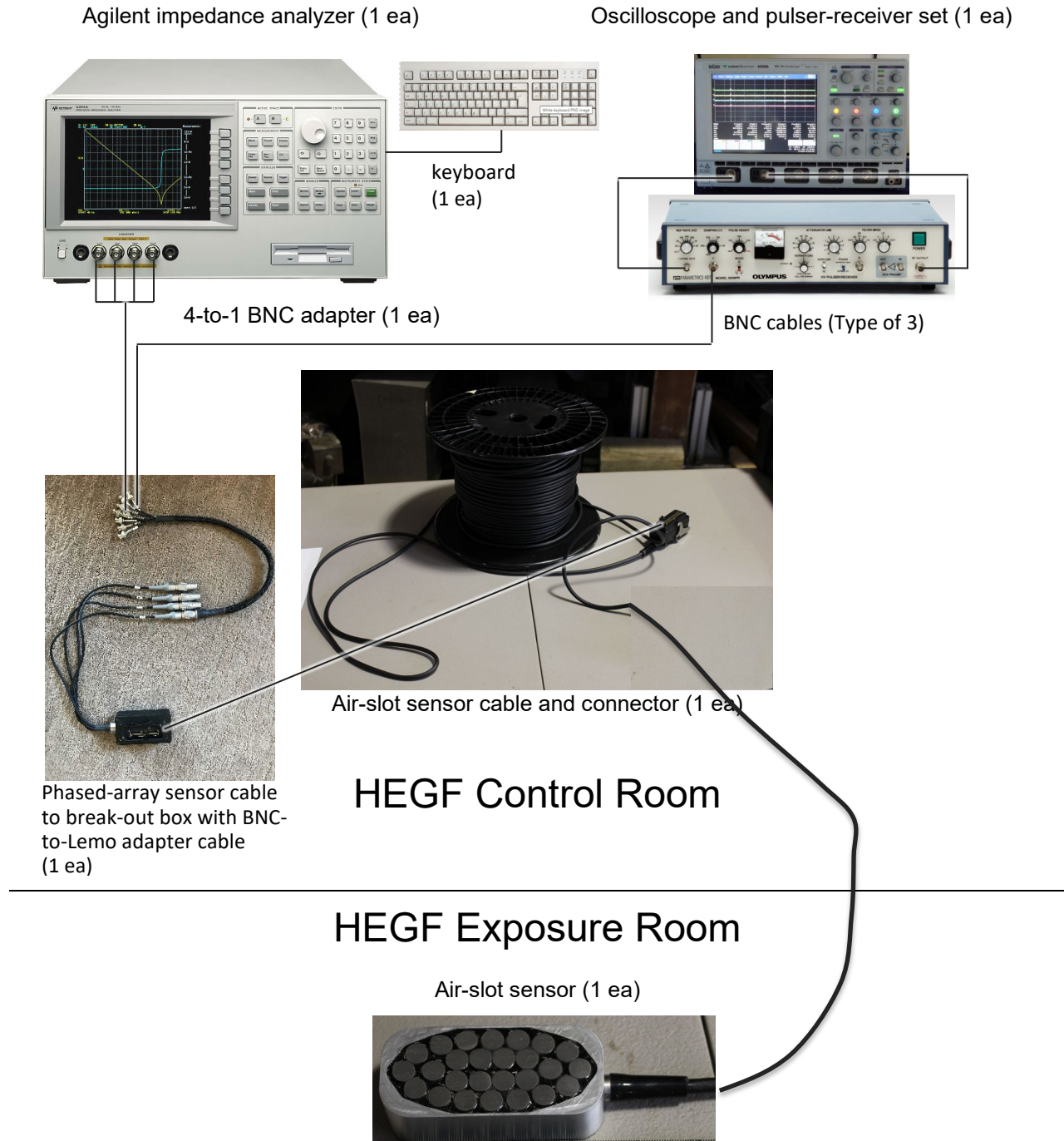


Figure 19. Diagram of air-slot sensor test equipment configuration in the HEGF Control Room.

The M&TE utilized for the piezoelectric air-slot sensor radiation tolerance robustness tests are listed in Table 4 (hardware). Photographs of equipment setups in the HEGF Exposure Room and Control Room are provided in Figure 20 through Figure 23.

Table 4. M&TE for the piezoelectric elements inside the air-slot sensor (hardware).

Equipment	I.D.#	Calibration Exp. Date	Application/Notes
Piezoelectric Sensor	GWPA-26-150-38.58-4E-OMNI-46	N/A	Sensor under test, provided by Guidedwave
Multichannel break-out box and BNC-to-Lemo adapter cable	N/A	N/A	Provided by Guidedwave
Agilent Precision Impedance Analyzer	Model 4294A, s/n JP2KG00998	N/A	Receives waveform signals from 24 of the Sensor components, and stores on disk
LeCroy Oscilloscope	Model LT342, s/n 01629	N/A	Displays pulse shapes and associated signals from each sensor element. Each printed using internal printer
Olympus High Voltage Pulser/Receiver	Model 5058PR, s/n 070060412	N/A	Used in tandem with Oscilloscope
Quincy Labs Mini Oven	Model 10AF s/n A1-2674	See Thermocouples	RAVIS components were within this Oven, which was within the Co-60 field
Oven TC/Module system	40007, 4009, 40011 Red Lion display	6/14/2021	Oven thermocouples and associated Red Lion readout module A
Data Logger for Oven temperatures	Model VC-TC s/n 103CC00180	N/A	Data Logging Oven temperatures
HEGF Timer	SWRC1-0002	03/2021	Provides minutes that Co-60 source is exposed

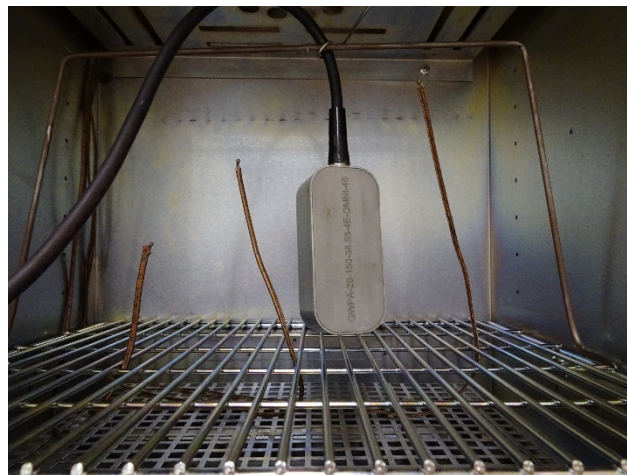


Figure 20. The piezoelectric air-slot sensor within the mini oven just prior to the start of irradiation at the 297 rad/hr dose rate.

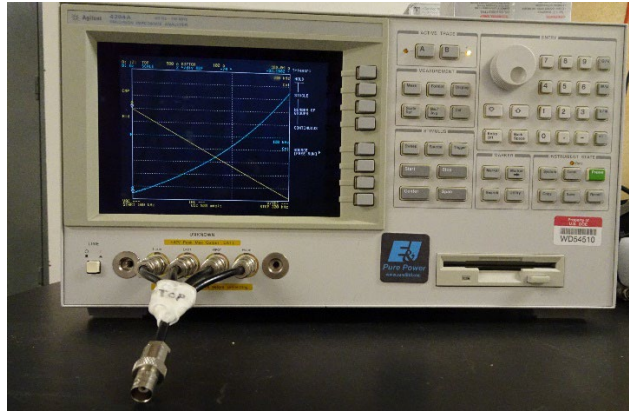


Figure 21. The Agilent Precision Impedance Analyzer Model 4294A, that receives waveform signals from 24 of the Sensor components and allows storage of this data on 3.5" computer disk.

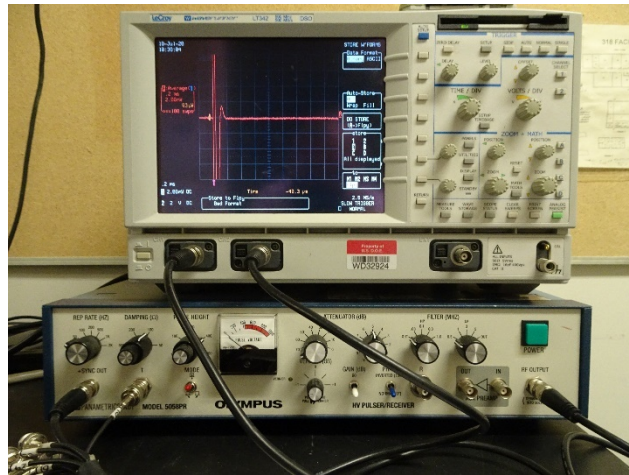


Figure 22. The LeCroy Model LT342 oscilloscope, and Olympus Model 5058PR High Voltage Pulser/Receiver, that is used in tandem with the oscilloscope.

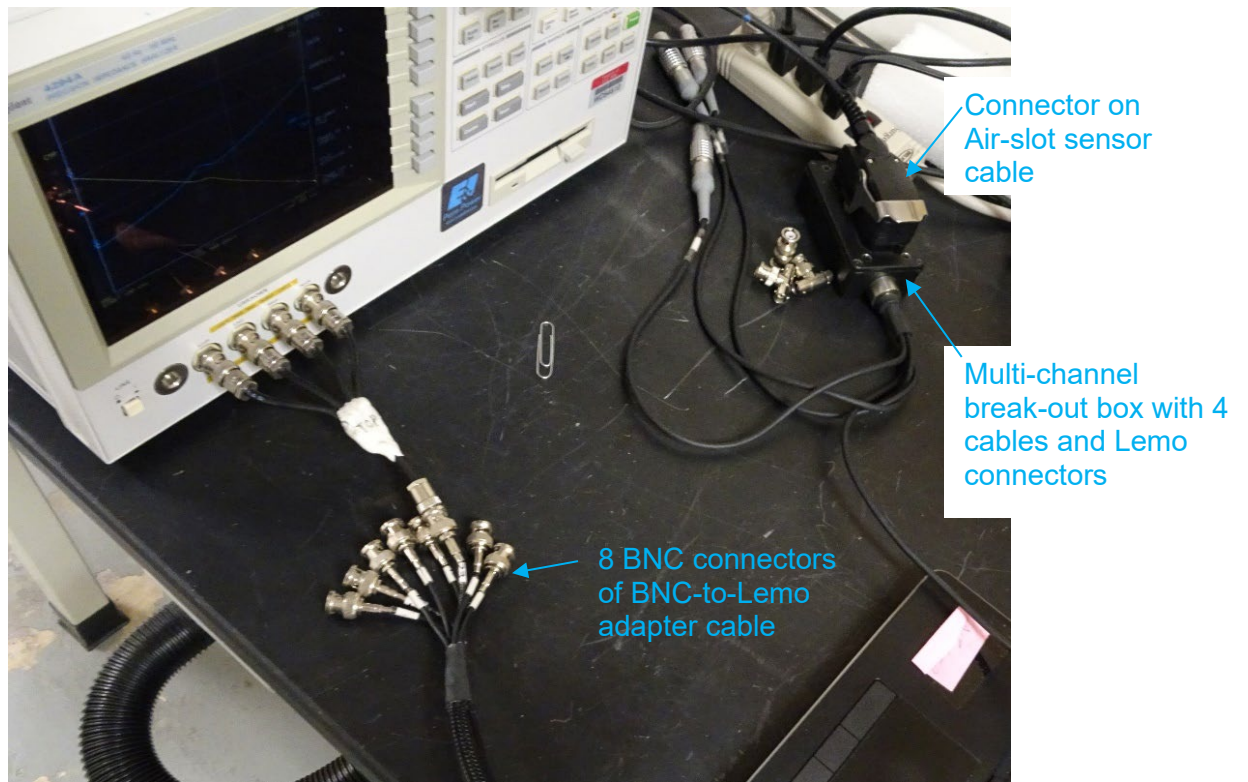


Figure 23. *Top:* Air-slot sensor cable connector plugged into the multichannel break-out box and interfaced with the impedance analyzer via a BNC connector on the BNC-to-Lemo adapter cable; *Bottom Left:* BNC-to-Lemo adapter cable with eight BNC connectors and one Lemo connector, which is connected to one of the four Lemo connectors from the multichannel break-out box in the photo; *Bottom Right:* Multichannel break-out box into which the air-slot sensor cable connected was connected to interface each of the sensor's piezoelectric elements with the test equipment.

6.0 Test Results and Discussion

6.1 PCB:DC Motor Pair Test Results

The radiation testing at elevated temperatures for the PCB:Motor pairs was executed from June 16 to June 20, 2020. General activities and observations associated with the PCB and DC motor testing, and corresponding dates and total doses, were recorded in the “Event Log,” a copy which is provided in Appendix III. As instructed in the Test Instruction, in addition to data recorded on the data sheets, screen shots of the Inuktun/Eddyfi ICON Diagnostics software outputs from the PCB:Motor pairs were saved to a shared drive for documentation of communication feedback from the software.

The main parameters/functions monitored and tested included observing PCB temperature, PCB voltage, PCB current, and spinning the motors forward and in reverse while observing the power supply current draw. Using the Test Instruction and associated data sheets, these specific test metrics were recorded. The observations showed that the current draw of the PCB:Motor pairs slowly increased over time. For the check at 54 hours (16.5 krad) it was observed that the current for all the PCB:Motor pairs had gone to zero and thus they were not functioning at all. However, upon opening the oven and the oven air temperature slowly decreasing to near room temperature, each PCB:Motor pair started coming back to life (power indicator lights came on). With the PCB:Motor pairs cooled to about 80-90°F, a check of the current showed the mA were back to normal; therefore suggesting the temporary failure was due to the continuous high temperature and not the radiation dose (see detailed discussion in the discussions section below).

After observing that the pairs functioned normally at 150°F, it was decided to obtain pair data at approximately 72°F before resuming testing at 150°F. After an additional 6.2 hours of radiation (18.2 krad total) and elevated temperature at this new 150°F, a data check found that pairs #1 and #4 had failed, and during data collection for the remaining pairs #2 and #3 they failed as well. Upon turning off the oven and the pair temperatures approaching room temperature, pair #4 came back to life, but the other pairs did not. Data was then collected for pair #4 at room temperature, the oven heated to a lower temperature of 100°F, and the irradiation resumed (after removing pairs 1-3 from oven). After an additional 20.5 hours of radiation (24.5 k rad total) and 100°F temperature, pair #4 was found unresponsive, and did not come back to life after cooling to room temperature. These events at the various temperatures and dose levels are captured visually in the plots in Figure 24, and in tabular form in Table 5. The PCBs were separated from their associated DC motors in order to allow continued irradiation and testing of the motors only.

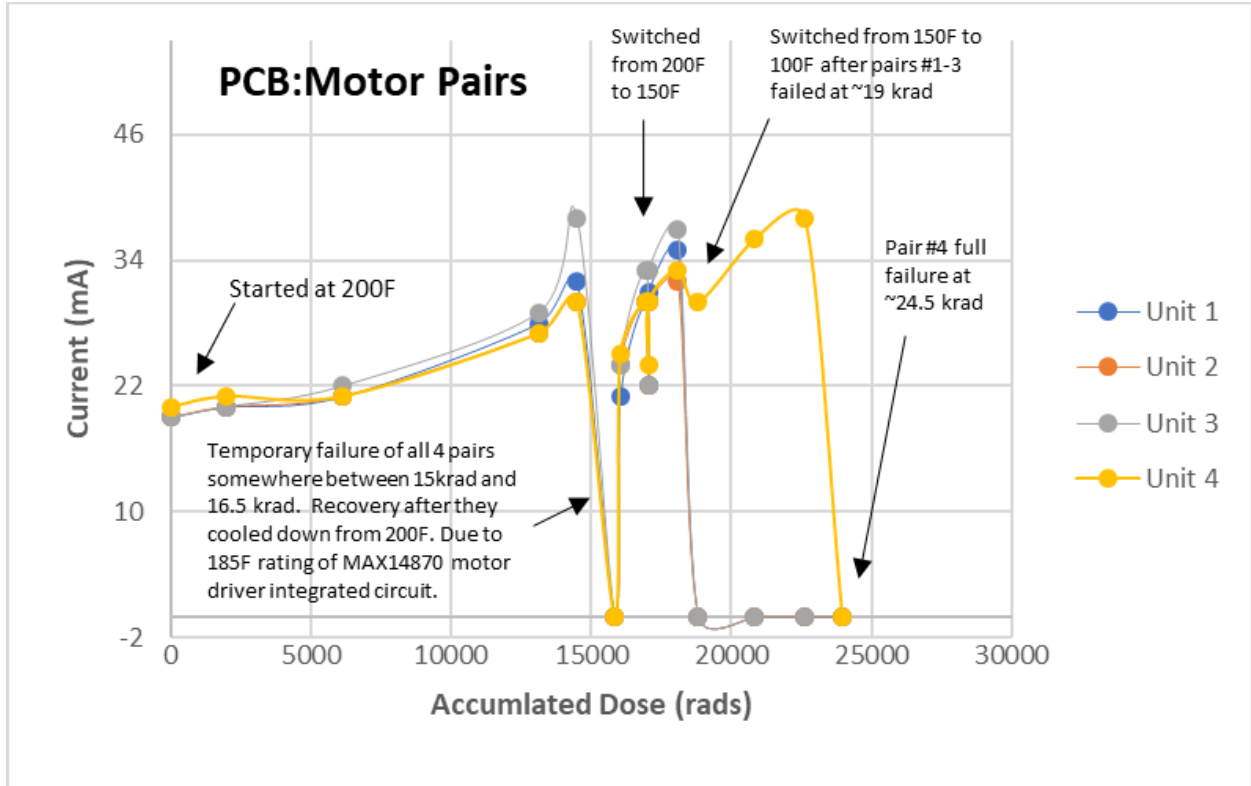


Figure 24. A plot of the PCB current reading (prior to spinning the motors) versus the accumulated dose. Provides visual representation of the effects of elevated temperature and increasing dose on the four PCB:Motor pairs, showing full failure at 19 krad for pairs #1-3, and full failure of pair #4 at ~24.5 krad.

Table 5. The Irradiation durations and dose levels at which symptoms were observed and measured for the various RAVIS components.

Duration and Dose Rate (hrs @ rad/hr)	Associated Radiation Dose (krad)	Oven Temp (F)	RAVIS Component	Symptom Observed*	Comments
0 @ 300	0.0	200	PCB:Motor #1	24.09V, 19mA, 34°C	Baseline data. Value for °C is from PCB board.
			PCB:Motor #2	24.06V, 19mA, 35°C	Baseline data. Value for °C is from PCB board.
			PCB:Motor #3	24.03V, 19mA, 35°C	Baseline data. Value for °C is from PCB board.
			PCB:Motor #4	24.04V, 20mA, 35°C	Baseline data. Value for °C is from PCB board.
54.0 @ 300	16.5	200	PCB:Motor #1	24.07V, 0.0mA, ~100°C	Found unresponsive but came back to life after temperature reduced.
			PCB:Motor #2	24.05V, 0.0mA, ~100°C	Found unresponsive but came back to life after temperature reduced.
			PCB:Motor #3	24.01V, 0.0mA, ~100°C	Found unresponsive but came back to life after temperature reduced.
			PCB:Motor #4	24.02V, 0.0mA, ~100°C	Found unresponsive but came back to life after temperature reduced.
48.8 @ 300	14.5	150	PCB:Motor #1	24.09V, 32mA, 99°C	The data collection done within about 10 hours of full failure of pairs 1-3.
			PCB:Motor #2	24.05V, 30mA, 101°C	The data collection done about 10 hours prior to full failure of pairs 1-3.
			PCB:Motor #3	24.02V, 38mA, 102°C	The data collection done about 10 hours prior to full failure of pairs 1-3.
			PCB:Motor #4	24.02V, 9-30mA, 99°C	The data collection done about 10 hours prior to full failure of pairs 1-3. Note mA fluctuating.
60.2 @ 300	19.0	150	PCB:Motor #1	24.07V, 0.0mA, ~100°C	Found unresponsive and did not come back to life after temperature reduced.
			PCB:Motor #2	24.05V, 0.0mA, ~100°C	Found unresponsive and did not come back to life after temperature reduced.
			PCB:Motor #3	24.01V, 0.0mA, ~100°C	Found unresponsive and did not come back to life after temperature reduced.
			PCB:Motor #4	24.02V, 0.0mA, ~100°C	Found unresponsive and DID come back to life after temperature reduced.

Duration and Dose Rate (hrs @ rad/hr)	Associated Radiation Dose (krad)	Oven Temp (F)	RAVIS Component	Symptom Observed*	Comments
80.7 @ 300	24.5	100	PCB:Motor #4	24.02V, 0.0mA, ~50°C?	Found unresponsive and did not come back to life after temperature reduced.
80.7 @ 300	24.5	200	Motor #1	12.01V and 9.0-9.5mA	Baseline for Motor-only prior to 2000 rad/hr phase. ~1 rps.
			Motor #2	12.02V and 9.0-9.5mA	Baseline for Motor-only prior to 2000 rad/hr phase. ~1 rps.
			Motor #3	12.02V and 9.0-9.5mA	Baseline for Motor-only prior to 2000 rad/hr phase. ~1 rps.
			Motor #4	12.03V and 9.0-9.5mA	Baseline for Motor-only prior to 2000 rad/hr phase. ~1 rps.
Added 137 @ 2000	300	200	Motor #1	12.02V and ~7.0 mA	Current had decreased from ~9.5 to ~7.0 mA, but motor still functioning at ~1 rps.
			Motor #2	12.02V and ~7.0 mA	Current had decreased from ~9.5 to ~7.0 mA, but motor still functioning at ~1 rps.
			Motor #3	12.02V and ~6.5 mA	Current had decreased from ~9.5 to ~6.5 mA, but motor still functioning at ~1 rps.
			Motor #4	12.02V and 7.5-8.0 mA	Current had decreased from ~9.5 to ~7.5 mA, but motor still functioning at ~1 rps.
0.0 @ 300	0.0	150	Sensor	See Appendix IV	Baseline.
226 @300	67.3	150	Sensor	See Appendix IV	Final data collection.

* The mA values are the initial current prior to spinning the motors. The Celsius values are from a thermocouple within the PCB board, so are reflective of the PCB temperature and not the ambient/oven temperature.

Upon permanent failure of the VT-50 PCBs, troubleshooting was undertaken to attempt to determine the exact cause. Starting with the input voltage location, the boards were probed for continuity until there occurred a discrepancy with regards to the components and their manufacturer-specified ratings and in comparing results from the control unit. Upon reaching the integrated circuit (IC) step-down regulator (part# LTC7103IUHE), it was noted that the output voltage was not as required (12 volts DC). To determine the possibility of failure of other upstream components, 12 volts was injected into the board where the step-down regulator had failed to do so. Upon doing this, all four PCBs responded with perceived full functionality, including functioning COM communication, ICON Diagnostics Communication, and motor control. It is important to note that, given the seemingly full functionality after bypassing the step-down regulator, it was not verified whether other PCB components had failed.

Therefore, it was determined that the *permanent* PCB failures were caused by this IC step-down regulator (part# LTC7103IUHE). The manufacturer's spec sheet for this IC indicates an operational range of -40°C to 125°C (104-257°F). The testing involved maximum temperatures of 93°C or 200°F, which is within the manufacturer's stated operational range.

6.2 Discussion of PCB:DC Motor Pair Test Results

The *temporary* failure of all PCB:DC motor pairs that was observed at around 16 krad during the 200°F phase (with immediate recovery after cooling) is believed to have been due to temperature alone. It is with relatively high probability that the component that caused this initial temporary failure is the Maxim MAX14870 motor driver integrated circuit. This component has an operational temperature limit of 85°C (185°F). What particular failure mechanism might have caused this at 200°F was not determined. This component does have thermal protection that will shut down the motor driver if it exceeds a certain temperature, but that temperature is 160°C (320°F). This is too high to do any good when operating at 200°F.

The data shown in Figure 24 indicate that the elevated temperatures have the effect of lowering the dose points at which *temporary* component failure occurs. However, it is not known whether the elevated temperatures have the effect of lowering the dose points at which *permanent* component failure occurs.

The LTC7103IUHE IC and the MAX14870 motor driver are COTS (commercial off-the-shelf) items, and not MIL (military) spec. They also are not believed to be of rad-hard classification. If the LTC7103IUHE IC in particular was replaced with one of a higher dose rating, and the MAX14870 motor driver was replaced with one of a higher temperature rating, the radiation dose level at which these PCBs would fail in temperature environments approaching 200°F could possibly be significantly extended.

The manufacturer's operational temperatures for the other main components on these particular PCBs indicated a maximum operational temperature of 125°C (257°F); therefore, 200°F temperatures should not be a problem for the rest of the components.

The total accumulated dose of 19-24 krad (1.9×10^4 - 2.4×10^4 rad) that is associated with the permanent failure of the PCB:DC motor pairs during this test can be compared to the dose levels in Table 6 (that were obtained from published literature). This table states that – for bipolar transistors, metal-oxide semiconductor field-effect transistor (MOSFET) transistors, many digital ICs, and crystal resonators – a dose level of 1×10^4 rad is related to a medium “probability negative effects will be observed” and that a dose level of 5×10^4 rad is related to a

med-to-high “probability negative effects will be observed.” Therefore, failure of the PCBs at this general dose level was not totally unexpected.

Table 6. Estimates of doses at which negative effects of radiation will likely be observed in the most radiation-sensitive electronic components within the RAVIS system; namely, Bipolar Transistors, MOSFET Transistors, Digital ICs (Si-Bipolar, SOS/SOI, Si-MOS, Si-CMOS), and Crystal Resonators.

A Photon Field (rad/hr)	B Approximate Dose Level (rad)	C Duration* in Field (hrs)	D Number of ** 8-Hour Deployments	Probability Negative Effects Will be Observed
50	1×10 ³	20	2.5	Low
	5×10 ³	100	13	Low to Med
	1×10 ⁴	200	25	Med
	1.5×10 ⁴	300	38	Med
	5×10 ⁴	1000	125	Med to High
	1×10 ⁵	2000	250	Very High
300	1×10 ³	3.3	0.4	Low
	5×10 ³	17	2.1	Low to Med
	1×10 ⁴	33	4	Med
	5×10 ⁴	167	21	Med to High
	6×10 ⁴	200	25	Med to High
	1×10 ⁵	333	42	Very High

* C=B/A ** D=C/8

The four PCBs were expected to fail at a total integrated dose in the range of 48-72 krad based on the results of 2018 radiation tolerance scoping tests with one PCB sample that was irradiated at a higher dose rate of 578 rad/hr and a lower nominal temperature of 77-98°F. The failure of three of four PCBs during the 2020 tests at a dose between 19.0 krad and 24.5 krad during irradiation indicates the compounding effects of heat and radiation accelerated PCB failure and reduced component life expectancy.

6.3 DC Motor Test Results

The DC motors were determined to still be fully functional after failure of all four PCBs and therefore irradiation of the lone DC motors resumed.

The radiation testing at elevated temperatures for the lone DC motors was executed from June 26 to July 02, 2020. General activities and observations associated with the PCB and DC motor testing, and corresponding dates and total doses, were recorded in the “Event Log,” a copy which is provided in Appendix III. Using the Test Instruction and associated data sheets, data was collected for each motor, including the volts and milliamps. A slow decrease in mA readings from approximately 9 mA to approximately 7 mA was observed over the irradiation period, but the DC motors continued to function until testing was terminated. The observation and results are tabulated in Table 5 and shown graphically in Figure 25.

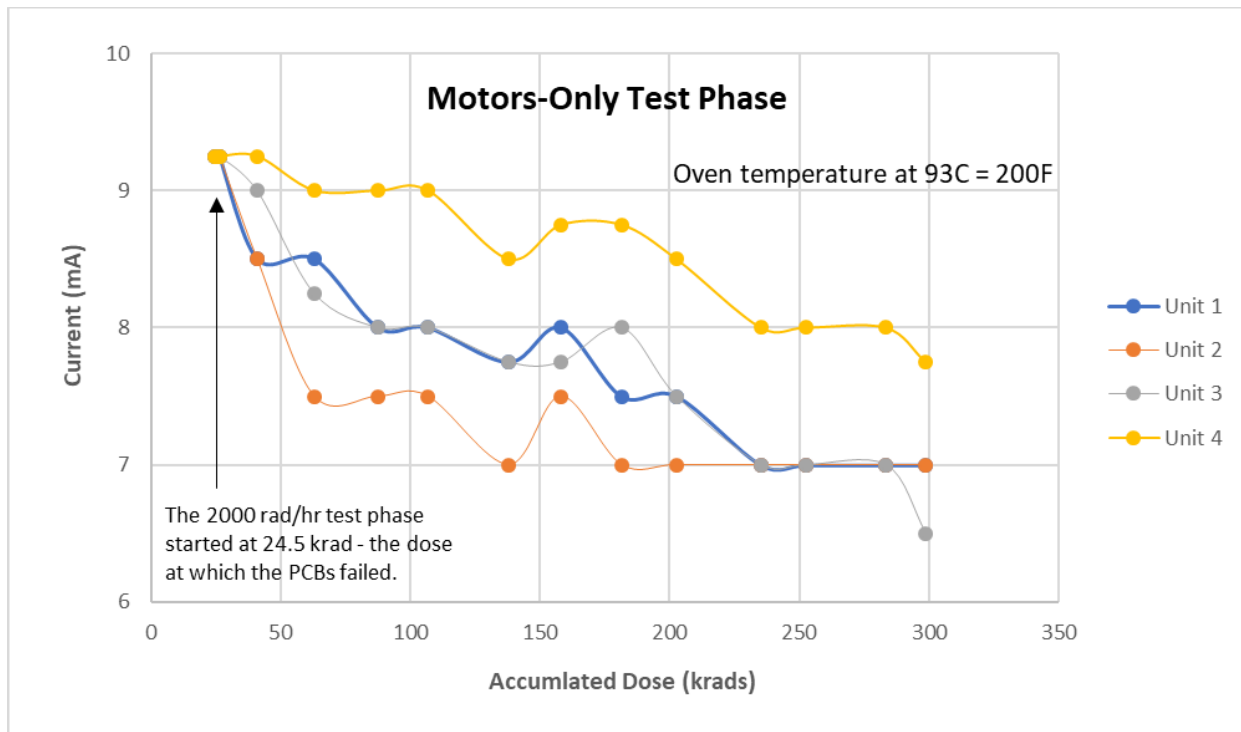


Figure 25. The current draw for the DC motors during the motor-only test phase (2000 rad/hr for a total of 299 krad), after the associated PCBs had failed at a dose between ~19 krad and ~24.5 krad.

6.4 Discussion of DC Motor Test Results

Based on the results of the 2018 radiation tolerance scoping tests, the DC motors were expected to fail at a cumulative dose beyond 72 krad. Figure 25 shows failure is likely to occur at a dose beyond 300 krad. The downward trend in current draw observed during 2020 testing indicates the DC motors may have been experiencing gradual failure as they approached the 300 krad test limit.

Extrapolation of the downward trend indicates a current draw of 0 amps would be reached at a total integrated dose of approximately 1 Mrad. The minimum current draw required for sensor kart actuation should be determined before a DC motor replacement interval is established. For example, if at least 7 amps are required to supply a coupling force of 150 lbs. (in an air-slot with debris), then the DC motor should be conservatively replaced before receiving a dose of 300 krad (approximately once every five years, assuming the 300 rad/hr dose rate) to reduce the likelihood of under-tank failure.

6.5 Air-slot Sensor Piezoelectric Element Test Results

The radiation testing at elevated temperatures for the air-slot sensor was executed from July 10 to July 20, 2020. Activities and observations associated with the air-slot sensor testing, and corresponding dates and total doses, were recorded in the “Event Log,” a copy which is provided in Appendix III. Using the Test Instruction and associated data sheets, data was monitored and recorded from 24 of the 26 sensor components/cells; namely, A18-A24, B17-B24, C17 and C19-C24, and D17 and D18. Although the intent was to collect response data

from all 26 piezoelectric elements available within the sensor (A17-A24, B17-B24, C17-C24, and D17 and D18), for reasons unknown, sensor elements A17 and C18 were found to not be functioning during baseline measurements prior to the start of irradiation. It was determined that resuming testing with only 24 elements (samples) was appropriate as 24 elements would be a representative sample size.

The impedance (ohms) vs. frequency (hertz) data collected at discrete dose intervals over the irradiation period were plotted together for each piezoelectric element, compared, and inspected for significant changes in impedance as a function of time and dose. An example plot containing all the impedance vs. frequency traces (and phase vs. frequency) for an element over the 10-day irradiation period is provided in Figure 26. Data collected on the last day (July 20) were collected at 150°F and 72°F, which are the black and orange traces, respectively. The impedance data for each of the 24 piezoelectric elements collected during the irradiation period are provided in graphical form in Appendix IV.

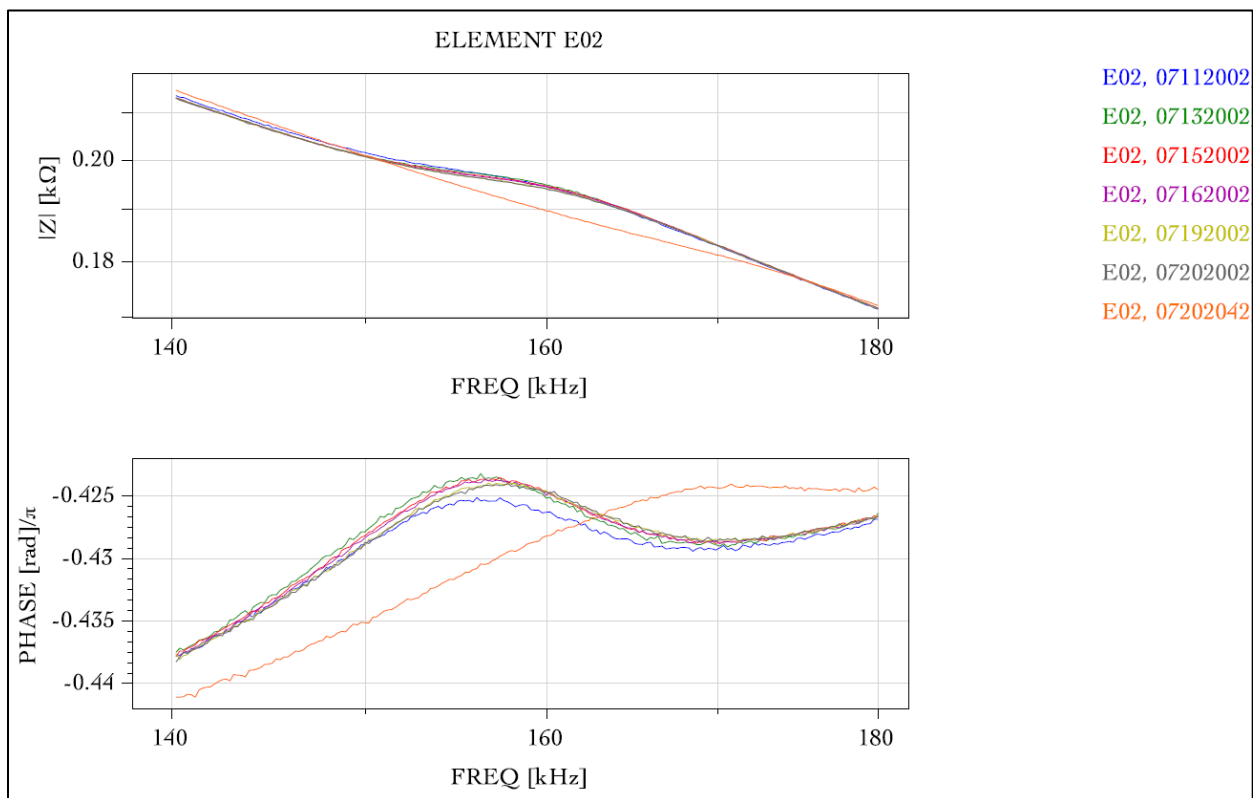


Figure 26. Top: Example of an impedance vs. frequency trace for piezoelectric element E02. Bottom: Example of an accompanying phase vs. frequency trace.

The baseline noise amplitude of the piezoelectric elements over the irradiation period was plotted, compared, and analyzed for significant changes in noise amplitude as a function of time and dose. A plot containing the baseline noise amplitude measurement data over the 10-day irradiation period is provided in Figure 27. The plot area shaded in light blue indicates the data that were collected while the air-slot sensor was undergoing irradiation. The unshaded portion of the plot indicates the data that were collected before irradiation started and after it had concluded.

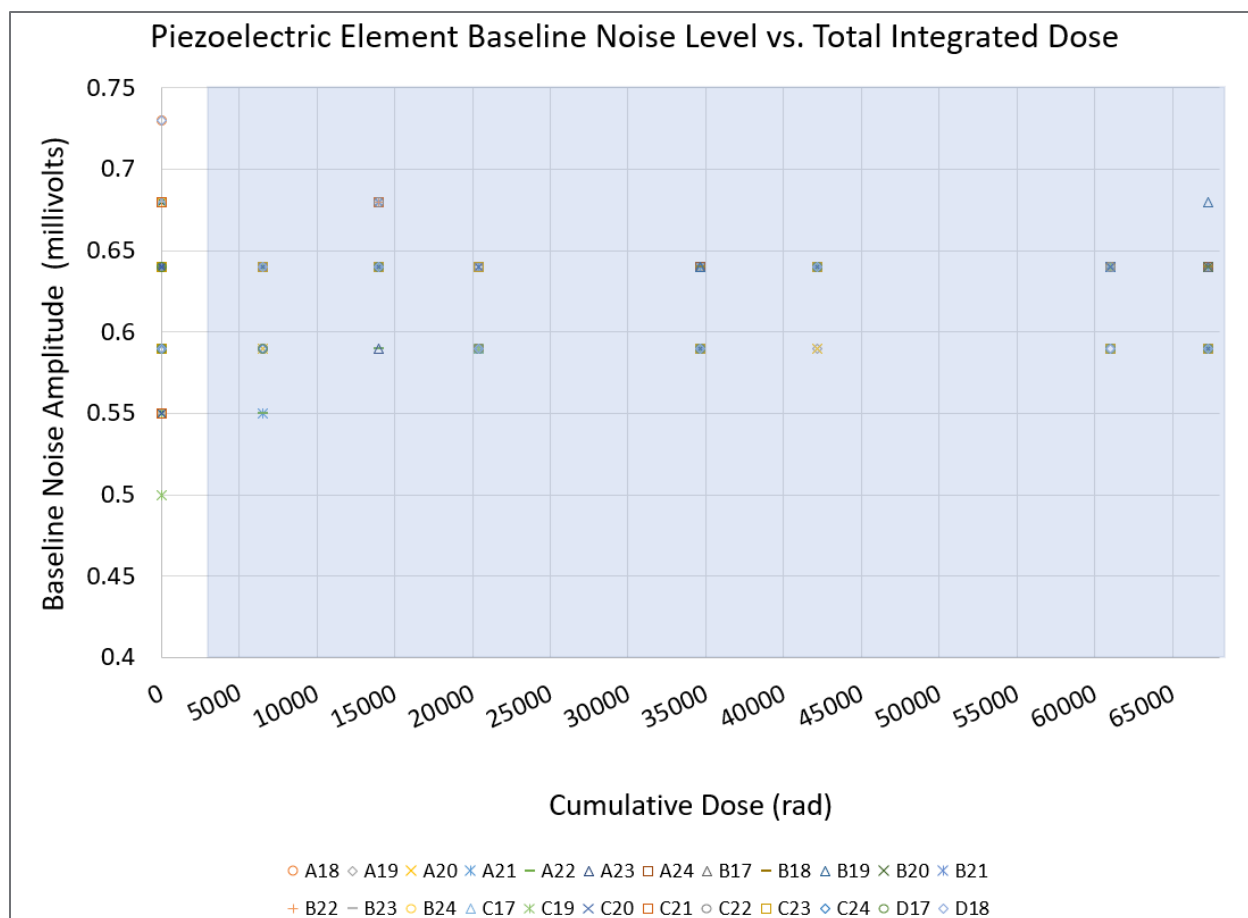


Figure 27. Baseline noise level (amplitude) of the air-slot sensor piezoelectric elements before starting irradiation (unshaded) and during irradiation (shaded in light blue).

6.6 Discussion of Air-slot Sensor Piezoelectric Element Test Results

Based on radiation tolerance literature values for components used in the construction of the air-slot sensor, the air-slot sensor was not expected to fail during irradiation to ~60 krad (the maximum dose expected after one year of service in the tank farms and the minimum life expectancy requirement placed on the sensor). The material in the sensor assembly that would likely fail first is the Teflon® material used in the cable jacket, insulation and separator material. Based on the range of dose tolerances reported in publicly available literature, this material is expected to fail between 100 krad and 5 Mrad, meaning it will last for at least 1.7 years of service in the tank farms, assuming the 300 rad/hr dose rate.

The goal of radiation tolerance testing for the air-slot sensor was to quantify the effects of gamma radiation on sensor signal quality, which affects flaw detection performance, by monitoring the electrical impedance and baseline noise level (amplitude) of the sensor's piezoelectric elements. The results of each measurement will be discussed here.

6.6.1 Impedance Results

In looking at the impedance plots in Appendix IV for piezoelectric sensor elements E02 through E26, in the frequency range from 140 to 180 kHz, the principal significant deviations in size of the resonance peak (nominally at 150 kHz but most often appearing at 160 kHz) appears to be in those traces corresponding to data recorded at significantly different operating temperature for the sensor, compared to the bulk of the traces. This typically shows up in these data plots as the orange or light blue traces, corresponding to the date of 07/20/20, and corresponding to sensor head temperatures of 72°F, or 22.2°C, compared to the 150°F or 65.5°C for nearly all the rest of the data traces.

Notwithstanding this, some deviations of peak height, position or general shape, do appear on certain references traces (dark blue) taken on the dates of 07/09/20 and 07/11/20, which were also taken at 150°F or 65.5°C. This, and certain other data that appear deviated from the average response taken from the bulk of the curves, appears consistent with less than optimal connections between the sensor element and the analyzer. These data traces together with those discussed above, for which it is likely that temperature differences are responsible for their deviation from the average response, are exempt from the following assessment.

The bulk of the traces taken during this testing (apart from those mentioned above) appear to move only slightly in phase, and very slightly in amplitude as a result of the radiation exposure. Specifically, the impedance amplitude response of this bulk of these curves appear to move on the order of 1% or less. This small a deviation in impedance amplitude of the piezoelectric sensor elements indicates little or no effective change in performance that can be ascertained through such an impedance analysis.

Furthermore, even if the impedance traces that appear further deviated from the bulk discussed immediately above are included, this further deviation being most likely due to temperature, the gross deviations of these traces are still only on the order of 5% and well within the $\pm 10\%$ test criteria. This deviation, even had it been due to radiation damage, would still not indicate that the sensor was unusable.

6.6.2 Baseline Noise Level Results

Inspection of the graph in Figure 27 shows the noise amplitude for all 24 of the piezoelectric elements was typically 0.59 mV or 0.64 mV. The change in amplitude during irradiation for each piezoelectric elements was within the $\pm 10\%$ test criteria with no evidence of increasing (or decreasing) noise level trends across the 10-day irradiation period, which means no significant changes in sensor noise level are expected to occur over a 10-day inspection campaign.

7.0 Summary and Conclusions

7.1 Summary

A set of RAVIS air-slot crawler inspection components were irradiated and tested in-situ to evaluate their gamma radiation tolerance. The components included PCBs and DC motors that represent drive system components in a RAVIS air-slot inspection crawler and an ultrasonic guided wave air-slot sensor containing 26 piezoelectric elements responsible for volumetric inspection of tank bottom plates.

The objectives of the radiation tolerance robustness tests were to:

1. determine the cumulative gamma doses at which the operational integrity of the PCB and DC motor robotic components become compromised and fail;
2. determine whether the baseline noise level (amplitude) of an ultrasonic guided wave air-slot sensor changes as a function of cumulative gamma dose while the sensor undergoes irradiation; and
3. generate tests results that:
 - a. support decisions on the cumulative dose at which preventive maintenance (component replacement) should occur for PCBs and DC motors to significantly reduce the likelihood of under-tank failure and the need for manual retrieval;
 - b. support decisions on whether the air-slot sensor can be expected to perform well under the effects of radiation and therefore whether it is suitable for under-tank deployment and whether signal quality observed in the lab during “cold” testing represents that which can be expected during under-tank deployments; and
 - c. provide a technical basis for determining the extent to which the air-slot sensor and robotic components satisfy radiation tolerance and lifecycle requirements S-9, S-10, UT-20, and R-24 from the Phase II requirements document “Technical Requirements for Sensor and Robotic Deployment System Maturation.”

In the absence of under-tank dose rate measurement data, nominal and upper-bound gamma dose rates of 50 rad/hr and 300 rad/hr were estimated for under-tank radiation conditions by tank farm subject matter experts. Radiation tolerance robustness tests were performed using a conservative but representative tank farm dose rate (297 rad/hr) and conservative but representative tank farm temperatures (150-200°F) for PCBs and DC motor robotic components to:

1. balance the cost of the tests with the value of the information gained, and
2. produce conservative failure doses to drive conservative component replacement intervals.

Radiation tolerance robustness tests with the air-slot sensor were performed at the same dose rate, but at a lower conservative representative temperature (150°F), which is the approximate maximum temperature tolerance of the weaker materials used in sensor construction (polymers/bonding materials).

In-situ tests were performed frequently during the component irradiation periods to generate high resolution failure doses and support evaluations of data trending over the irradiation period. Examination and analysis of the test data yielded the following:

- The PCBs functioned under the influence of gamma radiation and typically failed at a dose of 19 krad.
- The DC motors functioned under the influence of gamma radiation and did not fail during testing.
- The piezoelectric elements of the air-slot sensor functioned under the influence of gamma radiation and did not exhibit significant/perceivable changes in electrical impedance or baseline noise level (amplitude) over a 10-day irradiation period.

7.2 Conclusions

The test results support the following conclusions for each of the RAVIS components included in radiation tolerance robustness testing:

7.2.1 DC Motors

The DC motors can tolerate being actively irradiated at the conservative but representative 297 rad/hr dose rate at 200°F and can tolerate a cumulative dose of 300,000 rad, or that which would be incurred after 5 years of service at the 300 rad/hr dose rate. The component therefore meets minimum and preferred radiation tolerance and lifecycle requirements for robotic components. The minimum current draw required for sensor kart actuation in the RAVIS air-slot inspection crawler should be determined before a DC motor replacement interval is established. For example, if at least 7 amps are required to supply a coupling force of 150 lbs. (in an air-slot with debris), then the DC motor should be conservatively replaced before receiving a dose of 300 krad (approximately once every five years, assuming the 300 rad/hr dose rate) to reduce the likelihood of under-tank failure.

7.2.2 Air-slot Sensor

The air-slot sensor can tolerate being actively irradiated at the conservative but representative 297 rad/hr dose rate at 150°F and can tolerate a cumulative dose of over 60,000 rad, or that which would be incurred after 1 year of service at the 300 rad/hr dose rate. The sensor therefore meets minimum radiation tolerance and lifecycle requirements. It can be safely assumed that the sensor's flaw detection ability would not be compromised by radiation in the real under-tank operating environment. It can also be safely assumed that the baseline noise level observed during lab "cold" testing is representative of that which can be expected in under-tank conditions and, therefore, that the flaw detection observed in the lab is representative of that which can be expected during under-tank inspections.

7.2.3 PCBs

The PCB can tolerate being actively irradiated at the conservative but representative 297 rad/hr dose rate, but can only tolerate a cumulative dose of 19,000 rad at 150-200°F. The PCB does not meet minimum radiation tolerance and lifecycle requirements; however, because the component is considered replaceable, it can be preemptively replaced before a cumulative dose of 19,000 rad is reached, determined through either monitoring with a dosimeter or scheduled time intervals that are calculated based on conservative estimates of under-tank dose rates.

The PCB failure dose of 19,000 rad is considered conservative since it was obtained under high radiation dose rate and temperature levels, and on-board component failure dose may depend on dose rate (additional discussion on radiation-induced failure of electronics can be found in

Appendix V). However, a PCB replacement schedule that is dictated by the conservative failure dose would result in low likelihoods of under-tank failure and thus manual retrieval of an unresponsive air-slot inspection crawler. Less conservative failure doses could be determined for different combinations of lower dose rates and temperatures but would require extensive testing and samples and be of little value without under-tank dose rate measurements to calculate PCB replacement intervals in terms of service hours.

In the absence of under-tank dose rate data, two options for determining when to preemptively replace the PCB on an air-slot inspection crawler to mitigate the likelihood of under-tank failures are:

1. Monitor the cumulative number of hours a PCB in an inspection crawler has spent in service and replace the PCB when service time approaches 63 hours (failure time if a dose rate of 300 rad/hr is assumed) or 380 hours (failure time if a dose rate of 50 rad/hr is assumed), depending on risk tolerance. If a high dose rate near 300 rad/hr is assumed, then 63 hours of service would occur toward the end of one tank inspection campaign. If a nominal dose rate near 50 rad/hr is assumed, then 380 hours of service would occur toward the end of a fifth tank inspection campaign. Calculated PCB replacement intervals based on the typical PCB failure dose and the estimated nominal and upper-bound tank farm dose rates are provided in Table 6. The replacement intervals can be re-calculated if quantitative under-tank dose rate measurement data become available. This option will likely result in the most conservative (i.e., frequent) PCB replacements.
2. Add at least one small passive dosimeter to the air-slot inspection crawler and analyze the dosimeter(s) approximately once per year to quantify cumulative dose. The PCB could then be replaced when the cumulative dose approaches a threshold set somewhere below the 19,000 rad failure dose, depending on risk tolerance. This option would reduce conservatism associated with PCB replacement frequency.

Table 7. Calculated PCB replacement intervals in terms of service hours or quantity of tank inspections, based on the typical 19 krad dose at which PCB failure occurred during testing.

		Estimated Upper-Bound and Nominal Tank Farm Dose Rates	
		<i>300 rad/hr</i>	<i>50 rad/hr</i>
Dose at which Permanent PCB Failure Typically Occurs	<i>19 krad</i>	63 hours (0.8 tank inspections) ^a	380 hours (4.8 tank inspections) ^a

^a Assumes 80 hours are required to inspect one tank (based on an estimated 200 service hours per year and typical annual tank inspection rate of 2.5 tanks per year).

A parametric study involving a broad range of radiation/temperature combinations to obtain failure doses under less conservative gamma dose rate and temperature conditions would be expected to yield lower failure doses. However, such a study would require several test weeks and a large set of PCBs (and DC motors), the cost of which may not be warranted given the relatively low dollar value of the components and the relatively low level of hardship associated with preemptive component replacement. Also, failure doses obtained under less conservative conditions would be of little value without confident measurements of under-tank dose rates, which will be needed to calculate PCB failure time and replacement schedule.

The PCB and DC motor robotic components and the air-slot sensor are considered replaceable RAVIS components, meaning they can be swapped out without requiring a complete re-build of the RAVIS air-slot inspection crawler. All other RAVIS components not included in the scope of radiation tolerance robustness testing are considered low risk (i.e., their failure would not lead to high consequences) and therefore the investment of resources in determining the effects of radiation on their function/ performance or lifecycle was not warranted. The lifecycles of such sub-systems or components at dose rates of 50 rad/hour (rad/hr) and 300 rad/hr dose rates were coarsely estimated with calculations based on published radiation tolerance values for comparable sub-systems/components and an assumed 200 service hours per year. The lifecycles calculated for low-risk components can be used to set their replacement intervals.

Appendix I – DST Refractory Pad Temperature Data

Temperature data generated by thermocouples embedded in refractory pads beneath Hanford primary tanks were used to guide the selection of test temperatures for radiation tolerance robustness testing.

Refractory pad thermocouple data generated over the period of 2016 to 2018 were downloaded from the PNNL Hanford Online Environmental Information Exchange (PHOENIX) website in February 2018. The data for each double-shell tank (DST) were analyzed for, 1) the absolute maximum temperature recorded over the 2-year time period, and 2) the maximum average annual temperature recorded over the 2-year time period.

The bar graph in Figure I.1 shows the absolute maximum temperature (“highest maximum”) and the maximum average annual temperature (“highest average”) for all 28 tanks, ranked in order of highest maximum to lowest maximum temperature from left to right.

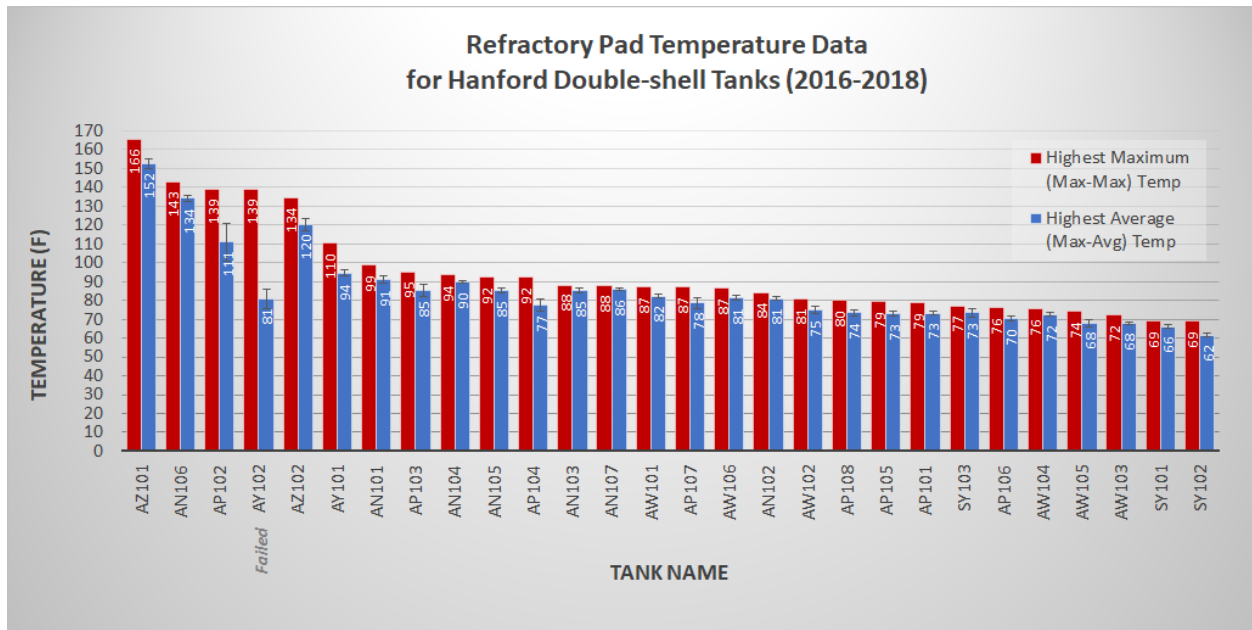


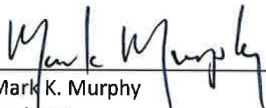
Figure I.1. Bar graph of the absolute maximum temperature and average temperature for each double-shell tank, as measured by refractory pad thermocouples.

Appendix II – Report of Calibration

REPORT of CALIBRATION – Dose and Temperature of RAVIS Robotics

Client: Kayte Denslow/PNNL PNNL Project: 75619	Tracking No.:	N/A
	Task:	Calibrations of Dose Rate of Co-60 source, oven temperature and accumulated dose to test items
	Measurement Dates:	June 14, 2020
	Final Report Date:	August 23, 2020

Measurements Performed and Reported by:

 8/23/2020

Mark K. Murphy Date
Engineer
Phone: (509)375-7331; Email: mark.murphy@pnnl.gov

Reviewed by:

 8/23/2020

Roman K. Piper Date
Engineer
Phone: (509)375-7339; Email: kim.piper@pnnl.gov

Introduction:

This report covers the calibrations involved for the dosimetry and elevated temperatures used for the RAVIS robotics (printed circuit boards (PCB) and motors) irradiations conducted within PNNL's High Exposure Facility (HEF) at Building 318 during the periods of June 16-20, June 26- July 2, and July 10-19, 2020. The associated dose rate and temperature measurements were conducted previously on June 14, 2020, within a Quincy Labs Model 10 mini-oven positioned within the beam of ^{60}Co source 318-545 (8450 curies at that time). These dose rate measurements were obtained using a calibrated *air-equivalent ionization chamber* (AEIC). The resulting rad/hour measurement, multiplied by the irradiation duration in hours, provides the desired total dose in rads. This report also covers the total integrated dose measurements obtained during the actual robotics irradiations, using *passive dosimeters*. These dosimeters were used as a secondary, or backup, for the ionization chamber/timer method. The calibrations of the thermocouples (TC) within the Oven were obtained in-place using a calibrated Type-J temperature standard. The associated Measurement and Test Equipment (M&TE) for these calibrations are provided in Table 1.

Table 1: Measuring and Test Equipment			
M&TE Item	S/N	Calibration Exp. Date	Application/Notes
Co-60 field within Oven	318-545	6/14/2021	Calibrated just prior to RAVIS testing
Exradin Model A12 Ionization Chamber	XA151686	7/23/2020	Used to calibrate dose rate of Co-60 field, in rad/hr.
Keithley Model 617 Electrometer	ECKE5-0004	03/2021	Used in conjunction with ionization chamber to record the ionization signal (amps).
Sunna Film Dosimeters	Batch 0399-20	1/13/2021	Placed in positions within field to measure integrated dose received by the RAVIS components.
Turner Trilogy Fluorimeter	7200-000341	1/13/2021	Used to analyze irradiated LiF films. Blue optics module s/n 7200-048 was used.
Quincy Labs Mini-Oven	Model AF-10 s/n A1-2674	See Thermocouples	RAVIS components were within this Oven, which was within the Co-60 field.
Oven TC/Module system	40007, 4009, 40011	6/14/2021	Oven thermocouples and associated Red Lion readout module A
Data Logger for Oven temperatures	Model VC-TC s/n 103CC00180	6/14/2021	Data Logging Oven temperatures
Type-J thermocouple standard	10815	12/11/2020	Used in conjunction with the Fluke Documenting Process Calibrator (DPC). Placed within the Oven to verify calibration of oven TCs at the 38°C, 65°C and 93°C points used for the testing.
Fluke Model 744 DPC Standard	24362	1/15/2021	Temperature readout DDPC used with Type-J TC
HEF temperature/pressure	WSCG1-0004	03/2021	Ambient conditions used to correct signal from ionization chamber.
HEF Timer	SWRC1-0002	03/2021	Provides minutes that Co-60 source is exposed

Co-60 Dose Rate Measurement Using an Air-Equivalent Ionization Chamber:

The radiation detector used to evaluate the dose rate was an Exradin Model A12 AEIC, which has an approximate sensitive volume of 0.24 cm³. The signal (electronic charge or current) from the ionization chamber is captured with a calibrated Electrometer. The Model A12 chamber and associated Electrometer can be seen in the photo in **Figure 1**. Since this signal from the vented ionization chamber is influenced by the ambient temperature and barometric pressure, a calibrated room thermometer and barometer were used to monitor measurement conditions. For the 300 rad/hr point, the mini-oven was centered at the 415 cm source distance and at 160 cm height above the floor (**See Figure 2**). For the 2000 rad/hr point, the mini-oven was centered at the 164 cm source distance and at 182 cm height above the floor (**See Figure 2**). The ionization chamber was positioned within the mini-oven at the center of the heating volume, and measurements were performed with the oven at ambient room temperature of 23-24°C. The Co-60 beam was attenuated to reduce the dose rate and allowed the 300

rad/hr position to be moved from the very back of the room to the 415 cm distance, thereby reducing the influence of room-backscattered gamma rays. The primary beam was incident upon the rear exterior surface of the oven (approximately 14.5 cm from the central reference position within the oven).



Figure 1. Shows the Keithley Electrometer Model 617 (left), and Exradin Model A12 ionization chamber with its buildup cap (right).



Figure 2: Shows dose rate measurement locations – in mini-oven at 415 cm source distance, attached to surface of oven, and at end of meterstick at 260 cm source distance.

Calibration of the A12 ionization chamber, within its buildup cap, was performed prior to these measurements using the 318 Building High Exposure Facility (HEF) ⁶⁰Co source 318-464. The absorbed dose rate to air (Air Kerma) was determined using the following equation:

$$\dot{K}_a = I_{ioniz} \cdot k_{TP} \cdot k_e \cdot N \cdot k_K \cdot 3600$$

- Where:
- \dot{K}_a is the average absorbed dose rate to air over the sensitive volume of the AEIC (commonly attributed to the position of the centroid of the chamber), in rad/h,
 - I_{ioniz} is the measured ionization current, in Amps (Coulombs/sec),
 - k_{TP} is the unitless correction for density of air within the AEIC volume,

- k_e is the unitless correction for the readout of the electrometer,
- N is the efficiency of the AEIC determined through comparison with the secondary transfer standard using the same photon energy, in R/C (Roentgen/Coulomb)
- $k_{K/X}$ is the conversion coefficient from exposure (Roentgen) to dose to air, expressed as Air Kerma (rad). A value of 0.879 was used, as referenced from ICRU 30 (1979), *Quantitative Concepts and Dosimetry in Radiobiology*,
- 3600 converts the time interval from seconds to hours.

The ambient temperature and barometric pressure, used for corrections in the ionization chamber signal, are taken from the calibrated room monitoring station. The irradiation duration is obtained using the calibrated timer on the HEF panel, and is multiplied by the measured dose rate to obtain the total integrated dose in rad.

Total Integrated Dose Measurements Using Sunna Dosimeters:

The client requested passive dosimetry be placed within the Co-60 field for the duration of the irradiations in order to provide verification that the source was exposed for the duration required, and that the oven/RAVIS components were always at the required location. Therefore, ideally the dosimeters would be located at the center of the oven. However, because the dosimeters used have a temperature dependency, they were instead positioned exterior to the oven at room temperature. The resulting positions were (1) 8.5 cm from the back surface of the oven, at the 392 cm source distance and 182 cm height above the floor, and (2) in air at the 260 cm source distance and 190 cm off the floor (secured to the end of a meter stick). This second location for passive dosimeters within a higher dose rate field was added in order to ensure any PCB component failures at dose levels lower than about 10,000 rad would be captured by the dosimeters. The dose rates at these two positions were measured with the A12 ionization chamber, which allowed ratios (correction factors) relative to the dose rate measured within the oven, and thus allowing correction of the dosimeters' readouts and accurate calculations for backup doses within the oven.

The Sunna film is microcrystalline LiF powder within a polyethylene matrix. The film dimensions are 1 cm x 3 cm with a thickness of 0.5 mm. The radiation energy is captured within the LiF storage phosphor, and the fluorescence read out signal (~530 nm, green) is induced by blue excitation light (~440 nm) – all provided by a *Fluorimeter*. Depending on the type of Fluorimeter, the dynamic dose response for the film can range from approximately 40 krad - 100 Mrad (0.4-100 kGy). The Sunna dosimeter films and Turner Designs Trilogy fluorimeter are shown in **Figure 3**. The readout value from the irradiated films (total counts obtained with a fluorimeter) is converted to dose, expressed as Air Kerma (kGy or krad) by using the calibration curve (see **Figure 4**). The calibration curve is generated from multiple films (with ~4 mm buildup jacket) irradiated to various dose levels within a calibrated Co-60 field.



Figure 3: The Sunna LiF film dosimeters (Left), and the Turner Trilogy Fluorimeter used to read out the dosimeters (Right).

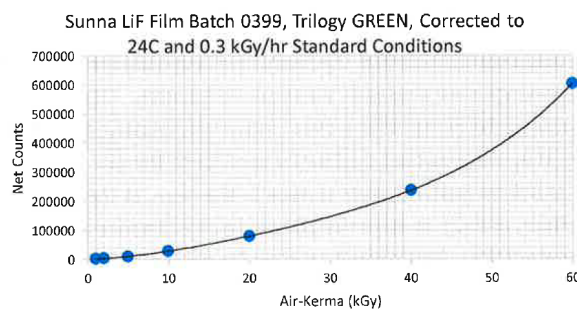


Figure 4: The Air Kerma Response Curve (Calibration curve) for the Sunna LiF film dosimeters, obtained with a calibration set of films irradiated within a calibrated Co-60 field. The curve is used to obtain a kGy value given the number of counts from film using the fluorimeter.

Oven Temperature Calibration:

The Quincy Labs Model 10 mini-oven, shown in **Figure 5**, was utilized for the elevated temperature testing within the Co-60 field. The three thermocouples positioned within the Oven volume are utilized for high-precision temperature control and monitoring. The center thermocouple (TC 40009, Red Lion display A) is used to control the oven temperature within about 1 °C, and the left (TC 40007, Input 1) and right (TC 40011, Input 5) thermocouples are used to monitor the oven temperature at low and upper heights, respectively. For this testing the thermocouple calibrations were performed at only the three temperature points used in the testing; namely, approximately 38°C, 65°C and 93°C (100°F, 150°F, 200°F) using a calibrated Type-J thermocouple temperature standard and a calibrated Fluke Model 744 readout standard (See **Figure 6**).



Figure 5. The interior of the Quincy Labs Model 10 mini-oven, showing the three thermocouples utilized for tight temperature control and monitoring. The center thermocouple is used to control the oven temperature within about 1 °C, and the left and right thermocouples are used to monitor the oven temperature at lower and upper positions.

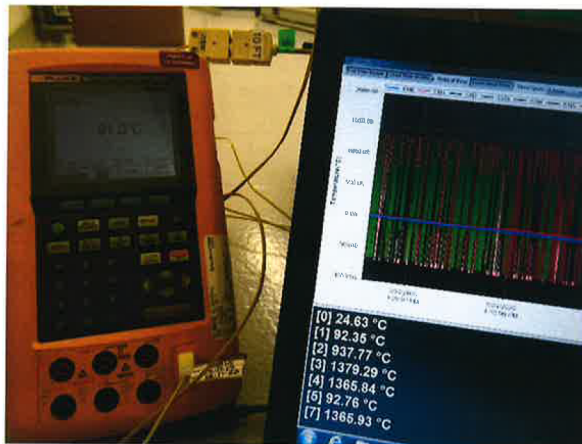


Figure 6. The calibrated Fluke Model 744 readout standard (Left), calibrated Type-J thermocouple temperature standard inserted into Oven port (Center), and the Data Logger display showing Inputs 1 and 5 on a laptop.

Dose Rate Measurement Results

Table 2 lists the dose rate results, both in terms of Air Kerma rate (rad/hr) and Exposure rate (R/hr) for cobalt-60 source 318-545.

Table 2. The dose rate measurement results obtained for cobalt-60 source 318-545, at Oven center and Dosimeter Locations outside Oven.

Location	Associated Source Distance (cm)	Associated Height off floor (cm)	Measured Air Kerma and Exposure Rate		Normalized to Oven Center*
			rad/hr	R/hr	
Center of oven volume	415	160	297	338	1.00
Dosimeter film position on exterior of oven	~390	160	364	414	0.816
Center of oven volume	162	180	2000	2275	1.00
Dosimeter film position on exterior of oven	~140	180	3140	3568	0.637

* These values are used to correct the film dosimeter values to obtain the associated total dose to PCBs and motors within the oven.

Table 3. The Total Accumulated Dose for various testing events, as determined with dose rate and irradiation time, as well as with passive dosimetry.

Irradiated Items	Oven/Item Source Distance (cm)	Event	Accumulated Dose in Air-Kerma (krad)	
			Per LiF Film*	Per DR and Time**
PCB:Motor Pairs	415	Temporary failure of all 4 pairs	15.4	16.5
PCB:Motor Pairs	415	Permanent failure of pairs 1-3	17.9	19.0
PCB:Motor Pairs	415	Permanent failure of pair 4	23.0	24.5
Motors Only	164	300 krad achieved	286	299
Sensor	415	Target dose achieved	62.7	67

* The 4-7% lower dose (as compared to ion chamber) measured with film was investigated and found to be attributed to a dose rate effect of the LiF film.

** Total accumulated dose as determined by multiplying the measured dose rate (DR) by the irradiation time. Because of lower uncertainty, these values should be used over passive dosimetry values.

Uncertainties

The estimated expanded uncertainty ($k=2$, 95% confidence level) for the accumulated dose values obtained with the ionization chamber and passive (film) dosimeters are 2.6% and 8%, respectively. These uncertainty estimates have been determined following the guidelines of Evaluation of Measurement Data – Guide to the Expression of Uncertainty in Measurement, JCGM 100:2008, and includes components evaluated by statistical means (Type-A uncertainties) and components determined on the basis of alternative methods, such as scientific judgment, calibration reports, etc. (Type-B uncertainties).

Appendix III - Event Logs for Testing of RAVIS PCBs, DC Motors and Air-slot Sensor

PCBs: Motor Pairs

RAVIS Robotics Radiation Testing – Event Log

By MIC Murphy

Facility: PNNL High Dose Gamma Facility Task: Irradiation of robotic components at elevated temperature

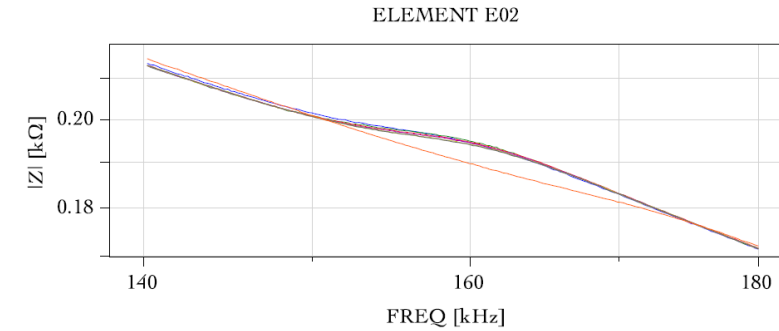
Date	Clock Time	Panel Timer Reading (min)	Spool Stack Sequence	Associated Integrated Dose	Notable Event/Comments
6/16/2020	~9AM	N/A	N/A	∅	Baseline data collection
"	~9:30AM	N/A	N/A	∅	Turned oven ON.
"	10:03AM	10,000	4,1,2,3	∅	Co-60 source UP to begin irradiation.
"	~5:10 PM	9602	4,1,2,3	2000 rad 2275 R	RAVIS data collection
6/17/20	~6:40 AM	8760	4,1,2,3	6262 rad 7124 R	RAVIS data collection.
6/17/20	5:06 PM	8192	4,1,2,3	9090 rad 10,341 R	RAVIS data collection
6/18/20	4:38 AM	7523	3,4,1,2	12,519 rad 14,242 R	stopped run to switch ^{spool} stack sequence to 3,4,1,2
6/18/20	7:30 AM	7350	3,4,1,2	13,383 rad 15,225 R	RAVIS data collection
6/18/20	12:06 P	7074	3,4,1,2	14,800 rad 16,800 R	RAVIS data collection
6/18/20	5:45 P	6761	3,4,1,2	16,500 rad 18,800 R	stand off RAVIS data collection
6/18/20	6:13 P	6735	3,4,1,2	16,500 rad 18,800 R	stopped run to check dead PCBs (all 4).
→ Shut off oven and opened oven door — PCBs slowly came back to life!!					
6/18/20	7:52 P	6735	3,4,1,2	same	Restarted after cooling PCBs. and oven now at 65.5°C = 150°F.
6/18/20	10:15 P	6590	3,4,1,2	17,200 rad 19,600 R	RAVIS data collect
6/18/20	10:51 P	6556	3,4,1,2	17,400 rad 19,800 R	Put source down and oven OFF for overnight
6/19/20	6:55 A	6556	3,4,1,2	same	RAVIS data collection at 24°C
6/19/20	7:45 A	6556	3,4,1,2	same	Turned oven ON for 150°F data.
6/19/20	10:48 A	6556	3,4,1,2	same	RAVIS data collection for 150°F/95°C
6/19/20	11:20 A	6556	3,4,1,2	same	Put source back up.
6/19/20	2:10 P	6390	3,4,1,2	18,200 rad 5000 20,700 R	RAVIS data collection — looking good.
6/19/20	~5 PM				Pairs 1 & 4 were failed when set arrived.
6/19/20	~5:30 PM	6187		19,200 rad 21,900 R	Pairs 2 & 3 failed too during Set's data collection.
6/19/20	6:07 PM	6153		19,200 rad 21,900 R	Murphy arrived to shut down source & oven.
→ Pair #4 came back to life during oven cooling... others dead.					
6/19/20	6:45 P	6153	3,4,1,2	same	collected data for Pair #4 at 24°C
6/19/20	7:50 P	6153	same	same	Restarted run for Pair #4 at 38°C = 100°F

1

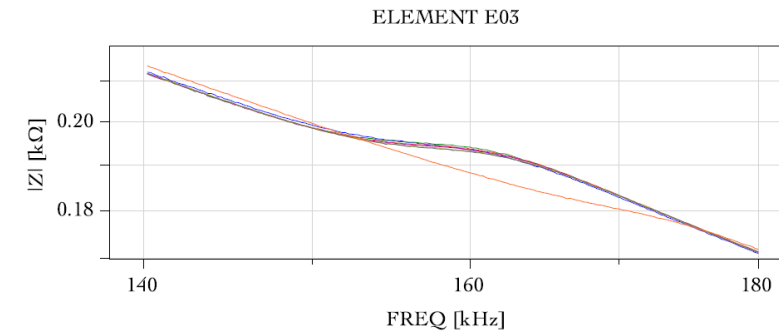
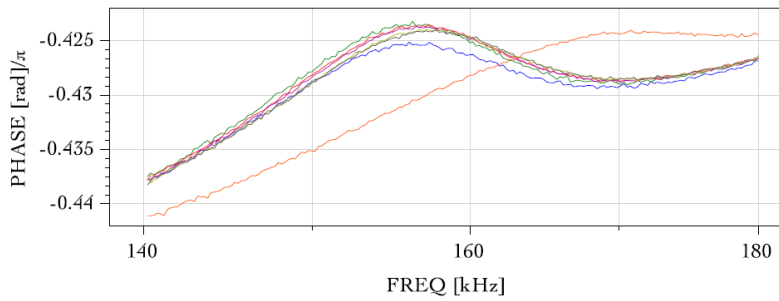
and after removing dosimeters at 160 & 415 cm locations, and removing Pairs 1, 2, 3. from oven.

Date	Clock Time	Panel Timer Reading (min)	Spool Stack Sequence	Associated Integrated Dose	Notable Event/Comments
6/20/20	2:05 AM	5790	3,4,1,2	21,200 rad 24,200 R	RAVIS data collection started for Pair #4
6/20/20	2:22 AM	5780	Same	Same	Put source up to resume run after down for temp check.
6/20/20	8:15 AM	5430	same		RAVIS Pair #4 data collection.
6/20/20	8:42 AM	5398	same		Source down for 10 min oven temperature check. 38°C
6/20/20	12:50 PM	5160	same	24,500 rad 27,800 R	Found Pair #4 @ 0.0 mA so shut source down and collected data.
					Shut oven OFF and cooled to 24°C. Pair #4 would not come back alive.
					Turned OFF power supply and removed Pair #4 from oven. Also removed film dosimeters.
					- Will now test Motors only, at 2000 rad/hr and 200°F
6/26/20	~12:30 P	10,000	3,4,1,2	24,500 rad 27,800 R	Started oven after taking Baseline data
6/26/20	12:53 P	10,000	3,4,1,2	same	Started Co-60 source one oven at 93°C = 200°F
6/26/20	1:45 P	9945	same	26,300 rad	Motor mA and mV check.
6/26/20	9:15 P	9505	same	41,000 rad	Motor mA and mV check, at Temperature.
6/27/20	8:15 A	8845	same	63,000 rad	Motor mA and mV check, and visual and temperature.
6/27/20	8:45 P	8106	same	87,600 rad	Motor mA and mV check.
6/28/20	6:18 A	7532	same	106,800 rad	Motor mA and mV check, and temp check and motor visual.
6/28/20	10:04 P	6597	2,3,4,1	137,900 rad	Motor mA and mV check. Temp and visual check.
6/29/20	8:13 A	5992	same	156,100 rad	Motor mA and mV check.
6/29/20	7:53 P	5292	same	181,400 rad	Motor mA and mV check, Temp and visual check too.
6/30/20	6:33 A	4655	same	202,700 rad	Motor mA and mV check, Temp and visual too. stuck shift
6/30/20	11:30 P	3677	1,2,3,4	235,300 rad	Motor mA and mV check, Temp and visual check too.
7/1/20	8:15 A	3160	same	252,500 rad	Motor mA and mV check, but accidentally left motors rotating 2 hrs!
7/1/20	11:42 P	2232	same	283,400 rad	Motor mA and mV check, Temp and visual check too. stuck shift
7/2/20	7:30 A	1770	same	299,000 rad	Motor mA and mV check, Motor visual and Temp. too. ~300 hrs
			- Testing	Complete	

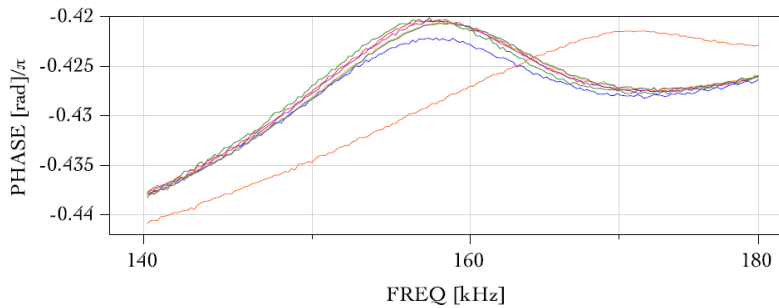
Appendix IV - Impedance Analyzer Data for the Piezoelectric Elements of Air-slot NDE Sensor

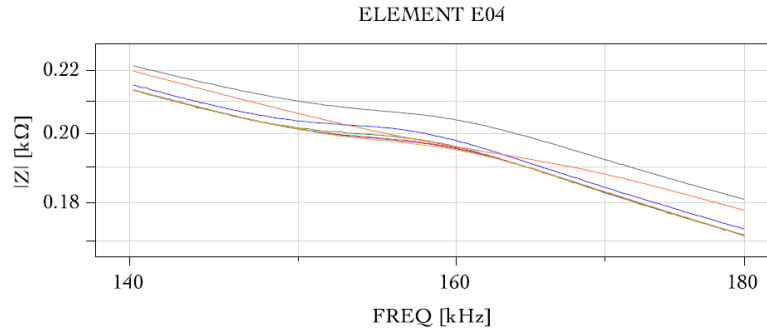


E02, 07112002, Disk 2, 07/11/20,
 E02, 07132002, Disk 3, 07/13/20,
 E02, 07152002, Disk 5, 07/15/20,
 E02, 07162002, Disk 6, 07/16/20,
 E02, 07192002, Disk 7, 07/19/20,
 E02, 07202002, Disk 9, 07/20/20,
 E02, 07202042, Disk 11, 07/20/20

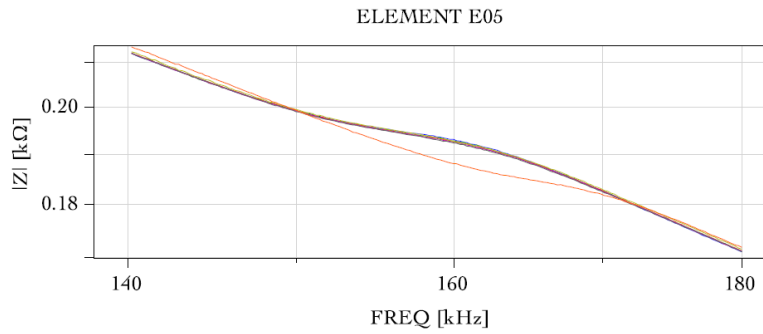
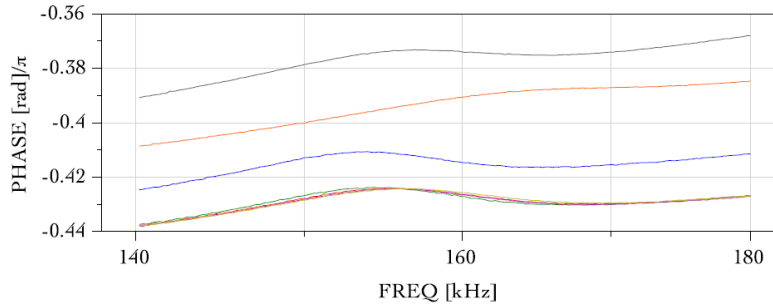


E03, 07112003, Disk 2, 07/11/20,
 E03, 07132003, Disk 4, 07/13/20,
 E03, 07152003, Disk 5, 07/15/20,
 E03, 07162003, Disk 6, 07/16/20,
 E03, 07192003, Disk 7, 07/19/20,
 E03, 07202003, Disk 9, 07/20/20,
 E03, 07202043, Disk 11, 07/20/20

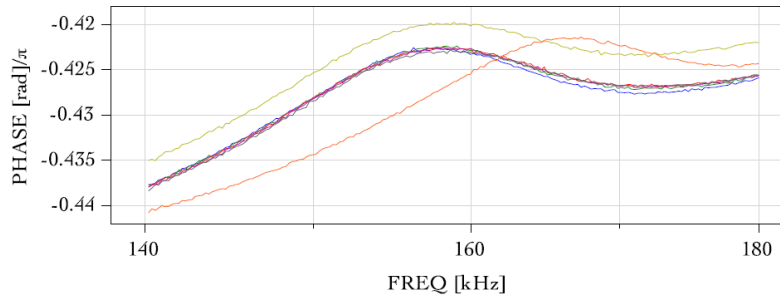


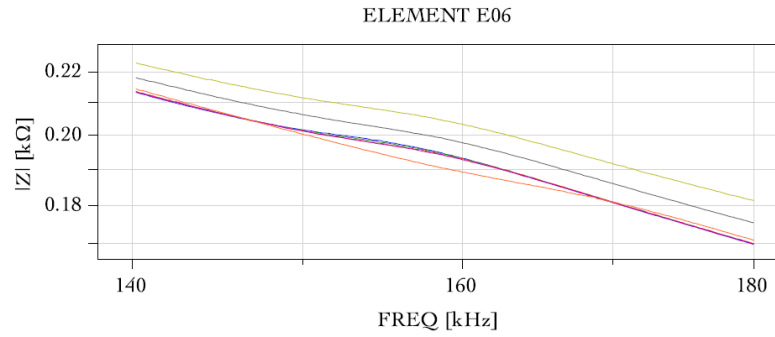


E04, 07112004, Disk 2, 07/11/20,
 E04, 07132004, Disk 4, 07/13/20,
 E04, 07152004, Disk 5, 07/15/20,
 E04, 07162004, Disk 6, 07/16/20,
 E04, 07192004, Disk 7, 07/19/20,
 E04, 07202004, Disk 9, 07/20/20,
 E04, 07202070, Disk 11, 07/20/20

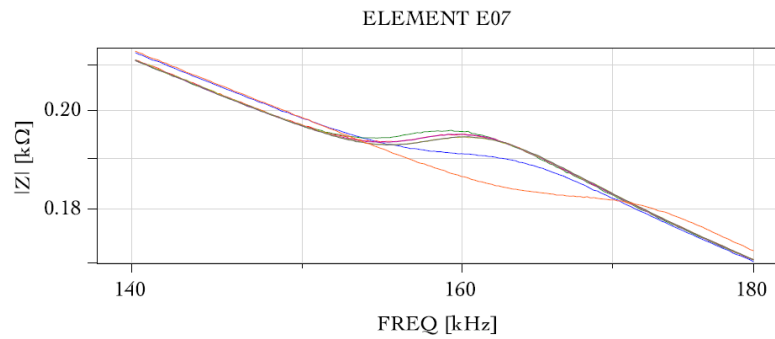
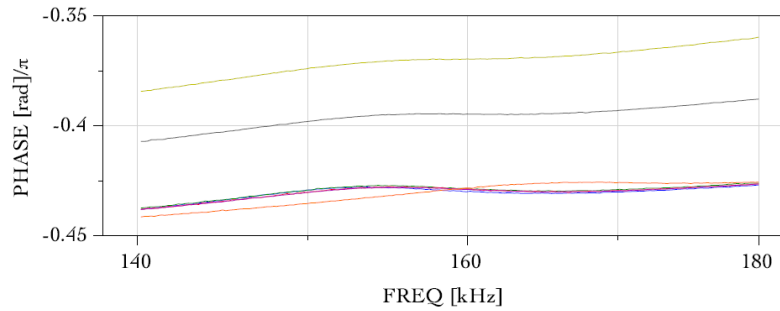


E05, 07112005, Disk 2, 07/11/20,
 E05, 07132005, Disk 4, 07/13/20,
 E05, 07152005, Disk 5, 07/15/20,
 E05, 07162005, Disk 6, 07/16/20,
 E05, 07192005, Disk 7, 07/19/20,
 E05, 07202005, Disk 9, 07/20/20,
 E05, 07202045, Disk 11, 07/20/20

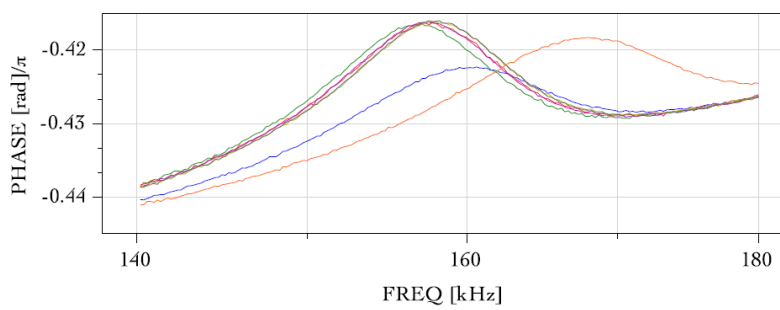




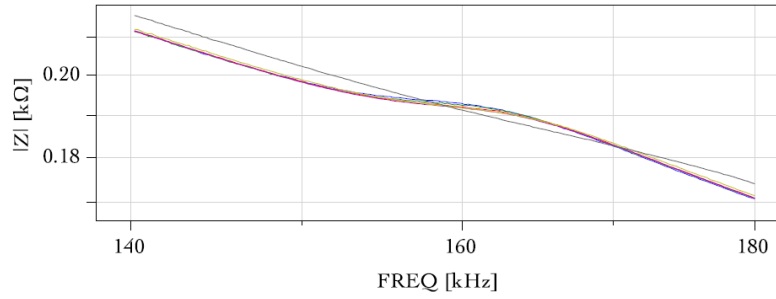
E06, 07112006, Disk 2, 07/11/20,
 E06, 07132006, Disk 4, 07/13/20,
 E06, 07152006, Disk 5, 07/15/20,
 E06, 07162006, Disk 6, 07/16/20,
 E06, 07192006, Disk 8, 07/19/20,
 E06, 07202006, Disk 9, 07/20/20,
 E06, 07202046, Disk 11, 07/20/20



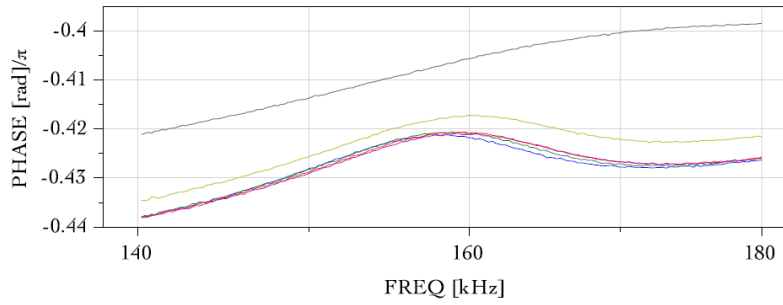
E07, 07112007, Disk 2, 07/11/20,
 E07, 07132007, Disk 4, 07/13/20,
 E07, 07152007, Disk 5, 07/15/20,
 E07, 07162007, Disk 6, 07/16/20,
 E07, 07192007, Disk 8, 07/19/20,
 E07, 07202007, Disk 9, 07/20/20,
 E07, 07202047, Disk 11, 07/20/20



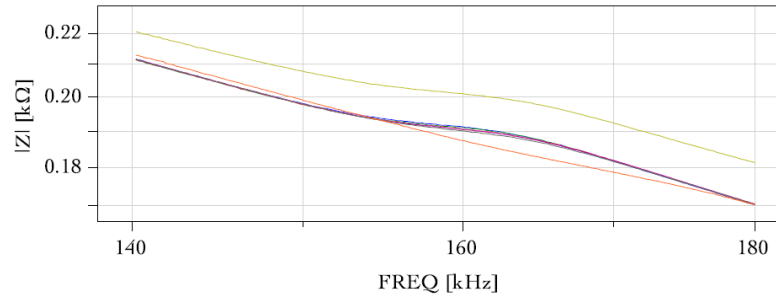
ELEMENT E08



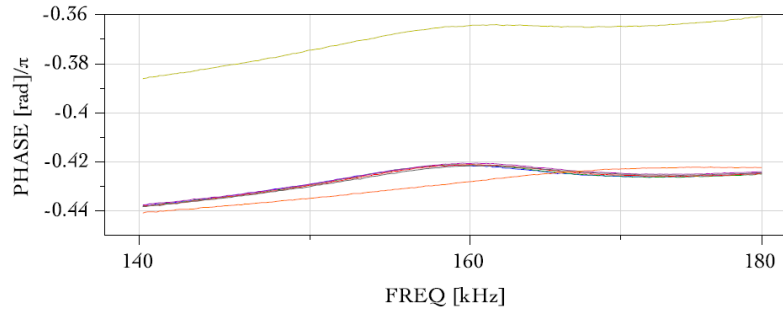
E08, 07112008, Disk 3, 07/11/20,
E08, 07132008, Disk 4, 07/13/20,
E08, 07152008, Disk 5, 07/15/20,
E08, 07162008, Disk 6, 07/16/20,
E08, 07192031, Disk 8, 07/19/20,
E08, 07202074, Disk 11, 07/20/20

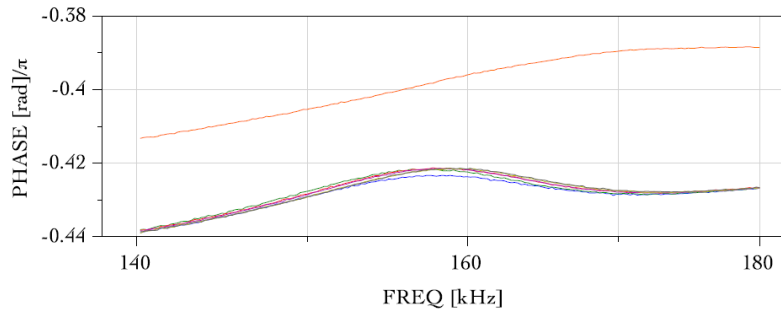
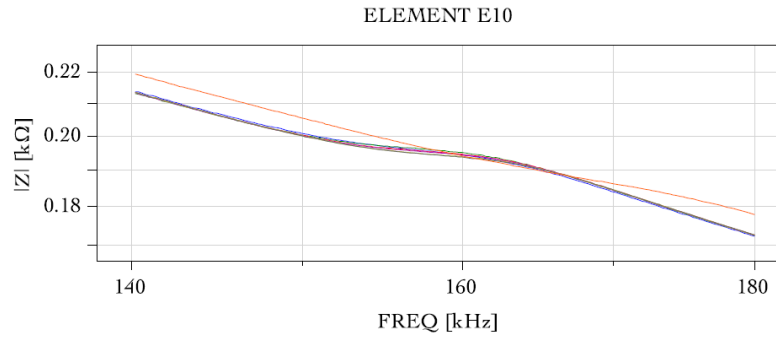


ELEMENT E09

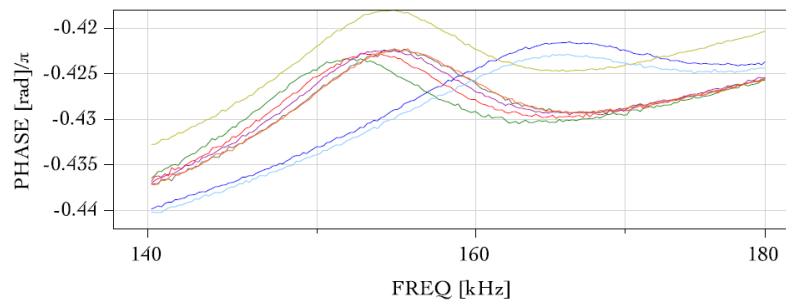
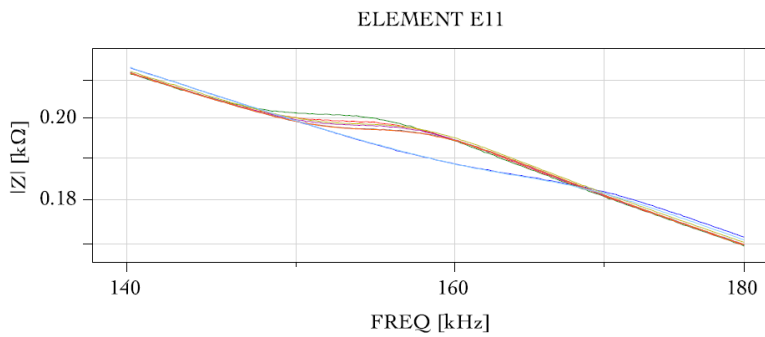


E09, 07112009, Disk 3, 07/11/20,
E09, 07132009, Disk 4, 07/13/20,
E09, 07152009, Disk 5, 07/15/20,
E09, 07162009, Disk 6, 07/16/20,
E09, 07192009, Disk 8, 07/19/20,
E09, 07202009, Disk 10, 07/20/20
E09, 07202049, Disk 11, 07/20/20



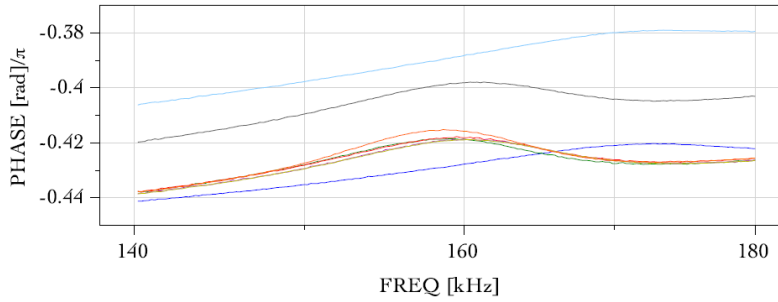
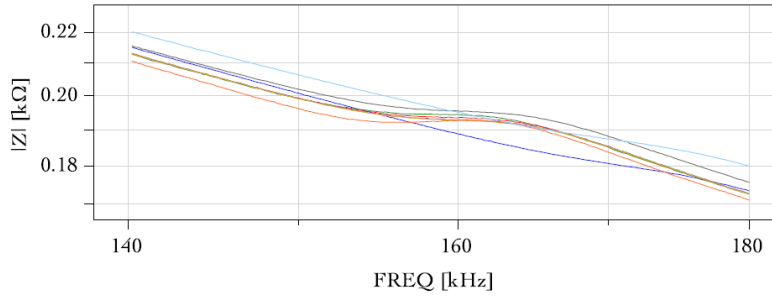


[E10, 07112010, Disk 3, 07/11/20,](#)
[E10, 07132010, Disk 4, 07/13/20,](#)
[E10, 07152010, Disk 5, 07/15/20,](#)
[E10, 07162010, Disk 6, 07/16/20,](#)
[E10, 07192010, Disk 8, 07/19/20,](#)
[E10, 07202010, Disk 10, 07/20/20](#)
[E10, 07202077, Disk 12, 07/20/20](#)



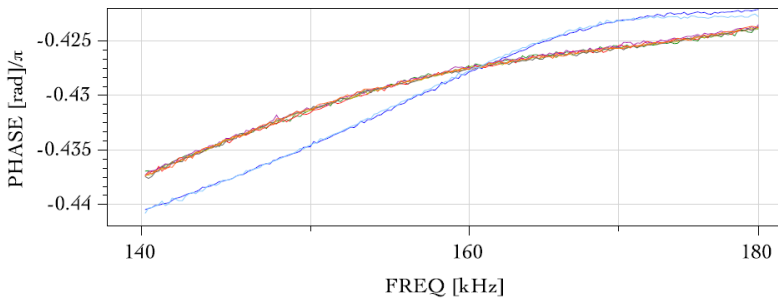
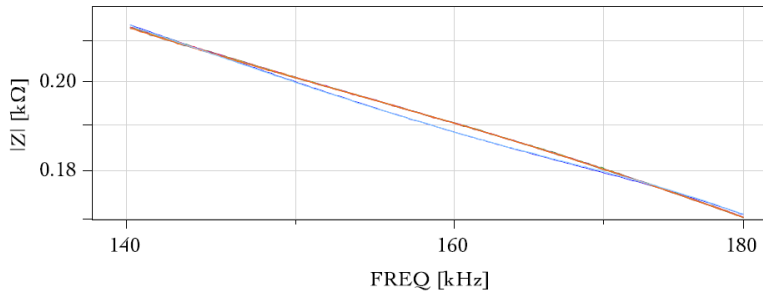
[E11, 06092011, Disk 1, 07/09/20,](#)
[E11, 07112011, Disk 3, 07/11/20,](#)
[E11, 07132011, Disk 4, 07/13/20,](#)
[E11, 07152011, Disk 5, 07/15/20,](#)
[E11, 07162011, Disk 6, 07/16/20,](#)
[E11, 07192011, Disk 8, 07/19/20,](#)
[E11, 07202011, Disk 10, 07/20/20](#)
[E11, 07202051, Disk 12, 07/20/20](#)

ELEMENT E12



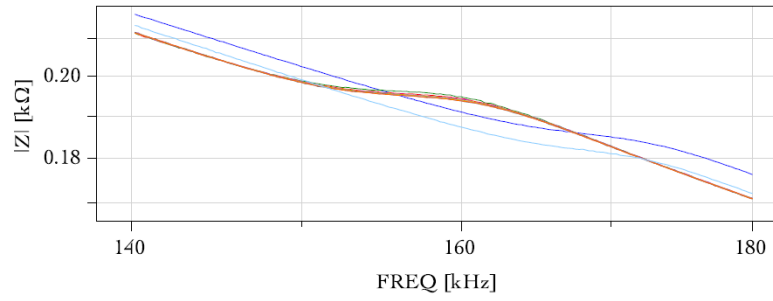
- E12, 06092012, Disk 1, 07/09/20,
- E12, 07112012, Disk 3, 07/11/20,
- E12, 07132012, Disk 4, 07/13/20,
- E12, 07152012, Disk 5, 07/15/20,
- E12, 07162012, Disk 7, 07/16/20,
- E12, 07192032, Disk 8, 07/19/20,
- E12, 07202023, Disk 10, 07/20/20
- E12, 07202079, Disk 12, 07/20/20

ELEMENT E15

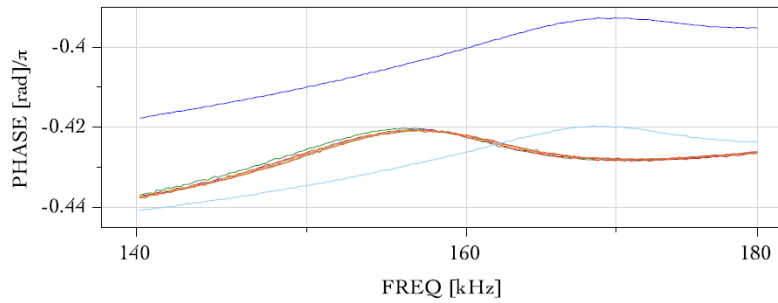


- E13, 06092013, Disk 1, 07/09/20,
- E13, 07112013, Disk 3, 07/11/20,
- E13, 07132013, Disk 4, 07/13/20,
- E13, 07152013, Disk 5, 07/15/20,
- E13, 07162013, Disk 7, 07/16/20,
- E13, 07192013, Disk 8, 07/19/20,
- E13, 07202015, Disk 10, 07/20/20
- E13, 07202053, Disk 12, 07/20/20

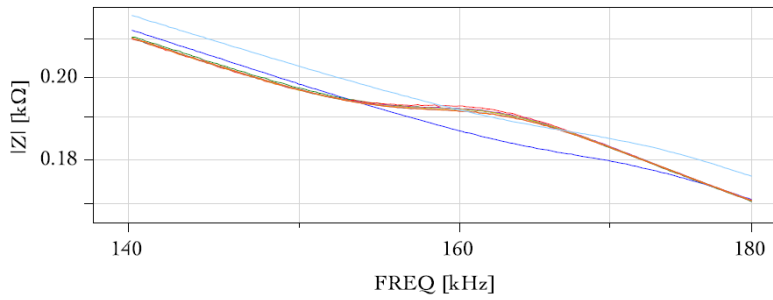
ELEMENT E14



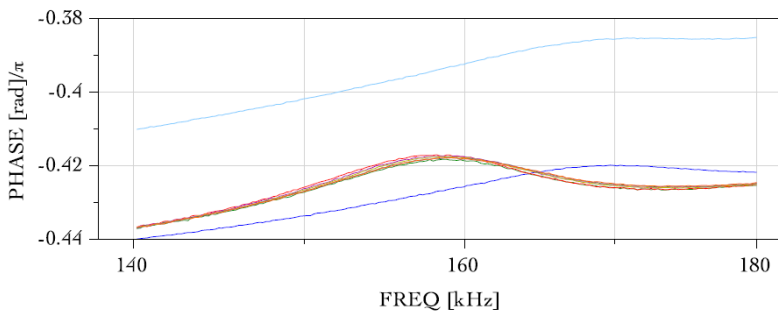
- E14, 06092014, Disk 1, 07/09/20,
- E14, 07112014, Disk 3, 07/11/20,
- E14, 07132014, Disk 4, 07/13/20,
- E14, 07152014, Disk 5, 07/15/20,
- E14, 07162014, Disk 7, 07/16/20,
- E14, 07192014, Disk 8, 07/19/20,
- E14, 07202014, Disk 10, 07/20/20
- E14, 07202054, Disk 12, 07/20/20



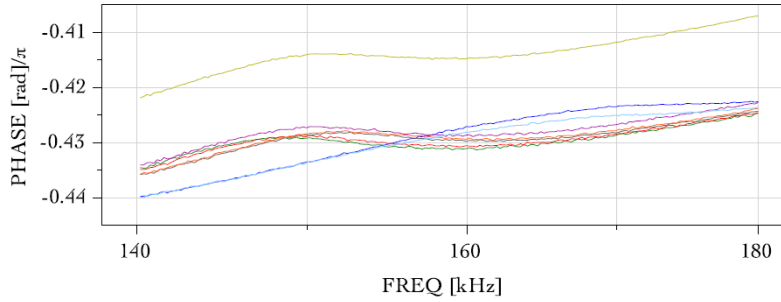
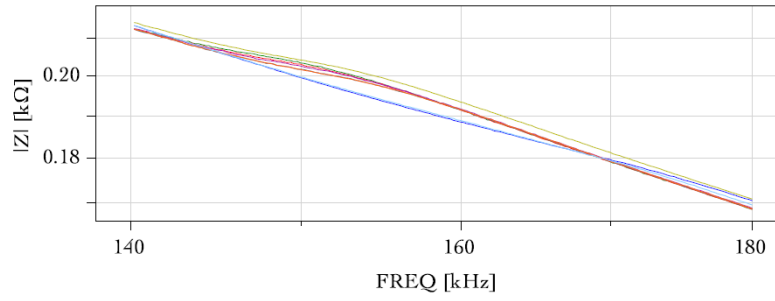
ELEMENT E15



- E15, 06092015, Disk 1, 07/09/20,
- E15, 07112015, Disk 3, 07/11/20,
- E15, 07132015, Disk 4, 07/13/20,
- E15, 07152015, Disk 5, 07/15/20,
- E15, 07162015, Disk 7, 07/16/20,
- E15, 07192015, Disk 8, 07/19/20,
- E15, 07202015, Disk 10, 07/20/20
- E15, 07202081, Disk 12, 07/20/20

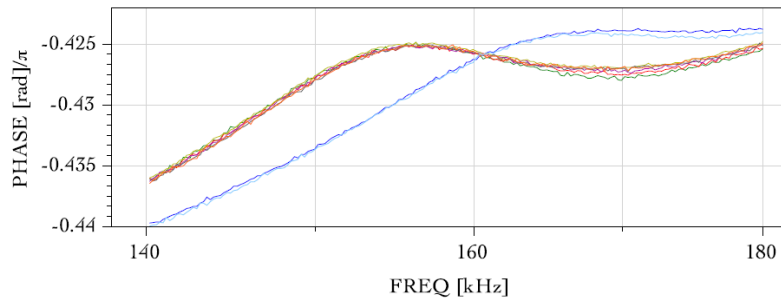
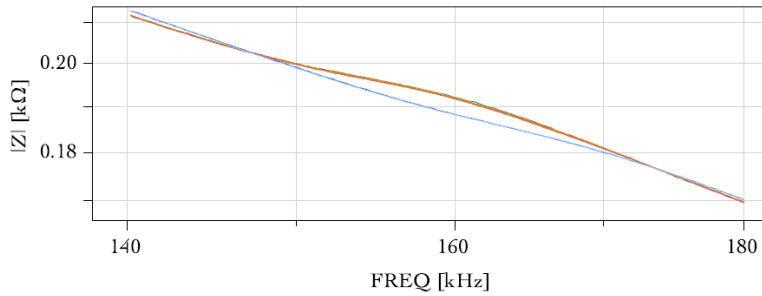


ELEMENT E16

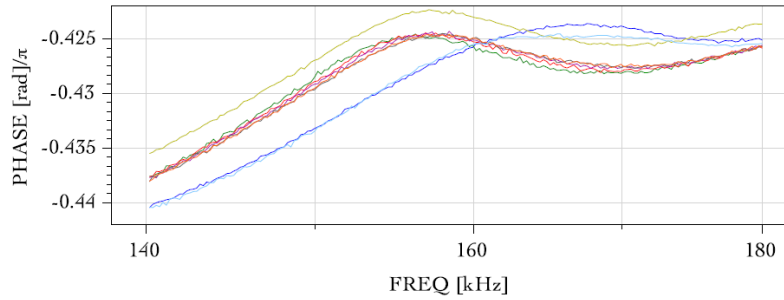
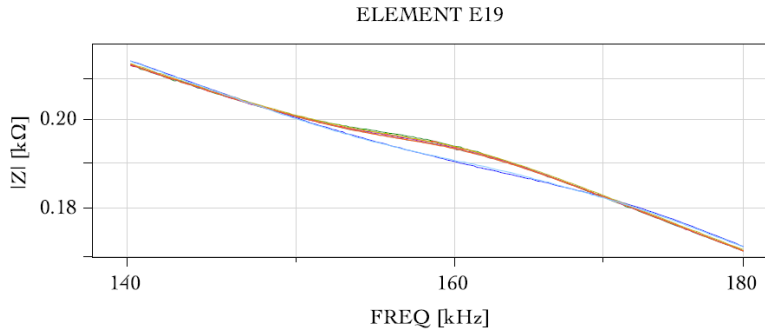


- E16, 06092016, Disk 1, 07/09/20,
- E16, 07112016, Disk 3, 07/11/20,
- E16, 07132016, Disk 4, 07/13/20,
- E16, 07152016, Disk 5, 07/15/20,
- E16, 07162016, Disk 7, 07/16/20,
- E16, 07192016, Disk 8, 07/19/20,
- E16, 07202016, Disk 10, 07/20/20
- E16, 07202056, Disk 12, 07/20/20

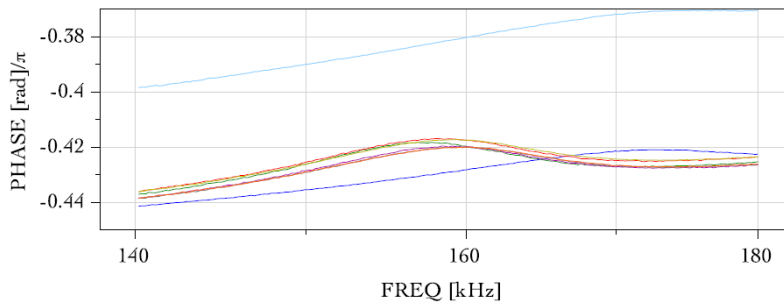
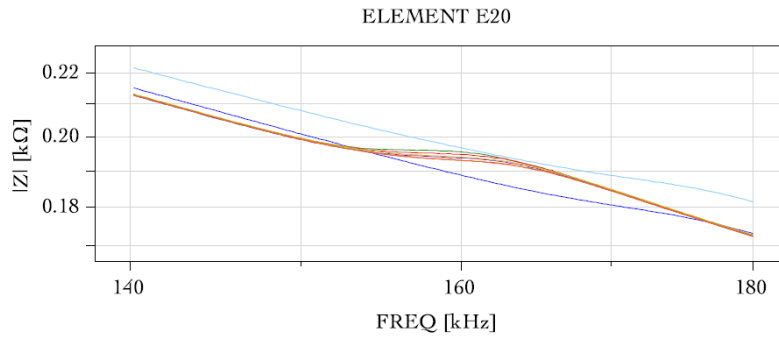
ELEMENT E17



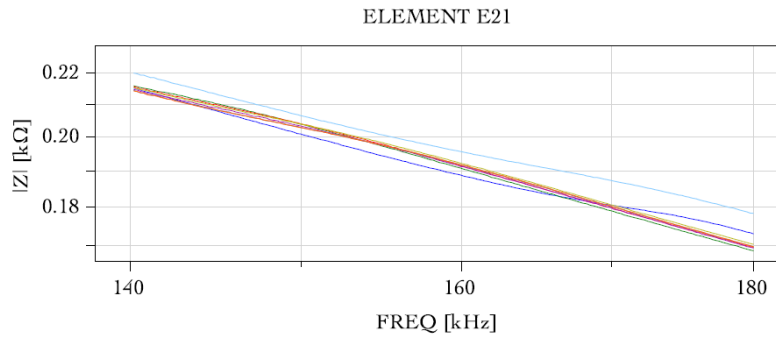
- E17, 06092017, Disk 1, 07/09/20,
- E17, 07112017, Disk 3, 07/11/20,
- E17, 07132017, Disk 4, 07/13/20,
- E17, 07152017, Disk 6, 07/15/20,
- E17, 07162017, Disk 7, 07/16/20,
- E17, 07192017, Disk 8, 07/19/20,
- E17, 07202017, Disk 10, 07/20/20
- E17, 07202057, Disk 12, 07/20/20



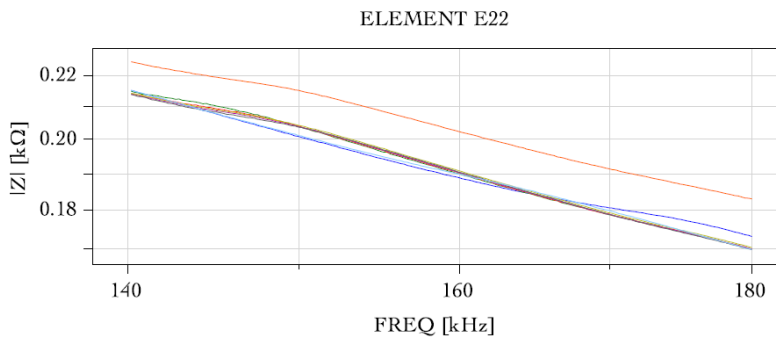
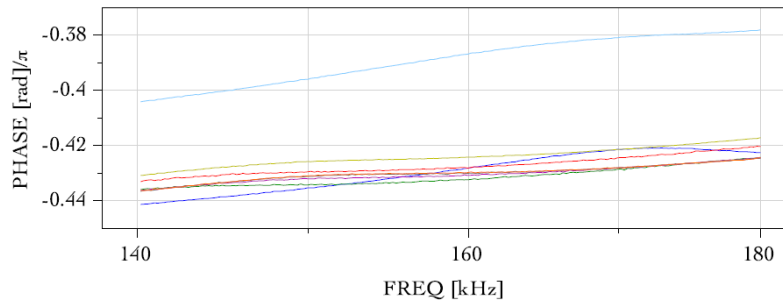
- [E19, 06092019, Disk 1, 07/09/20,](#)
- [E19, 07112019, Disk 3, 07/11/20,](#)
- [E19, 07132019, Disk 4, 07/13/20,](#)
- [E19, 07152019, Disk 6, 07/15/20,](#)
- [E19, 07162019, Disk 7, 07/16/20,](#)
- [E19, 07192019, Disk 8, 07/19/20,](#)
- [E19, 07202019, Disk 10, 07/20/20](#)
- [E19, 07202059, Disk 12, 07/20/20](#)



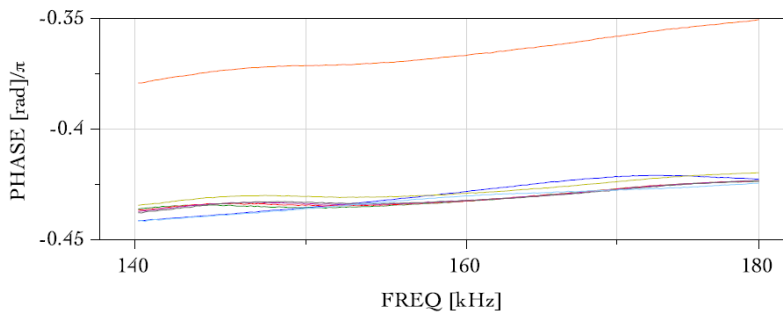
- [E20, 06092020, Disk 2, 07/09/20,](#)
- [E20, 07112020, Disk 3, 07/11/20,](#)
- [E20, 07132020, Disk 4, 07/13/20,](#)
- [E20, 07152020, Disk 6, 07/15/20,](#)
- [E20, 07162020, Disk 7, 07/16/20,](#)
- [E20, 07192020, Disk 8, 07/19/20,](#)
- [E20, 07202020, Disk 10, 07/20/20](#)
- [E20, 07202060, Disk 12, 07/20/20](#)



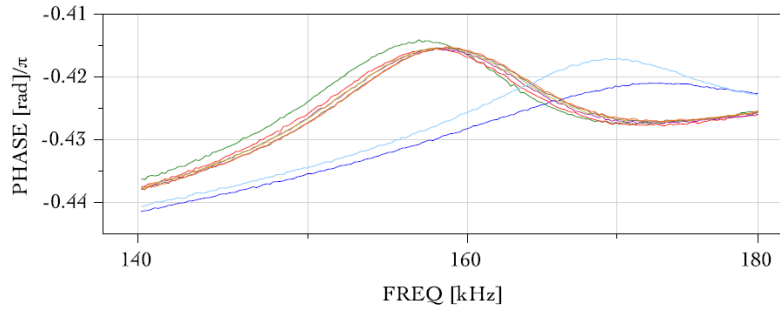
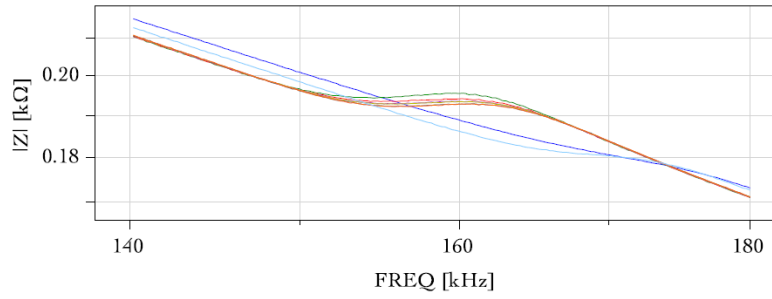
- E21, 06092020, Disk 2, 07/09/20,
- E21, 07112021, Disk 3, 07/11/20,
- E21, 07132021, Disk 4, 07/13/20,
- E21, 07152021, Disk 6, 07/15/20,
- E21, 07162021, Disk 7, 07/16/20,
- E21, 07192021, Disk 9, 07/19/20,
- E21, 07202021, Disk 10, 07/20/20
- E21, 07202082, Disk 12, 07/20/20



- E22, 06092020, Disk 2, 07/09/20,
- E22, 07112022, Disk 3, 07/11/20,
- E22, 07132022, Disk 4, 07/13/20,
- E22, 07152022, Disk 6, 07/15/20,
- E22, 07162022, Disk 7, 07/16/20,
- E22, 07192022, Disk 9, 07/19/20,
- E22, 07202035, Disk 10, 07/20/20
- E22, 07202062, Disk 12, 07/20/20

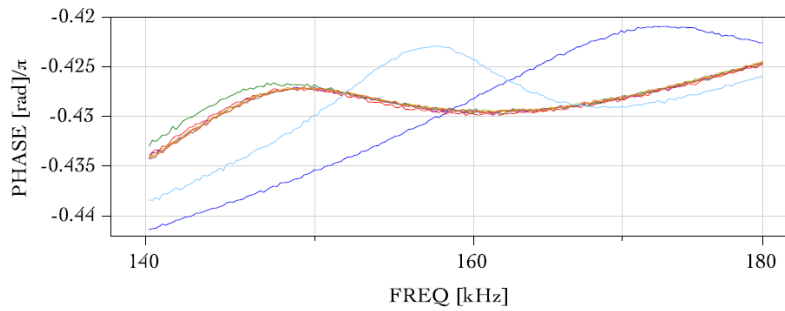
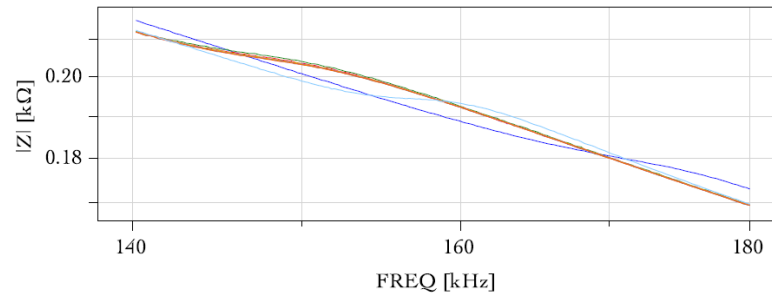


ELEMENT E23

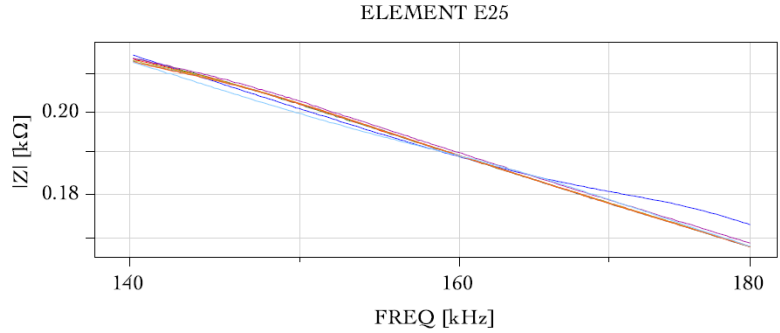


- E23, 06092020, Disk 2, 07/09/20,
- E23, 07112023, Disk 3, 07/11/20,
- E23, 07132023, Disk 5, 07/13/20,
- E23, 07152023, Disk 6, 07/15/20,
- E23, 07162023, Disk 7, 07/16/20,
- E23, 07192023, Disk 9, 07/19/20,
- E23, 07202023, Disk 10, 07/20/20
- E23, 07202063, Disk 13, 07/20/20

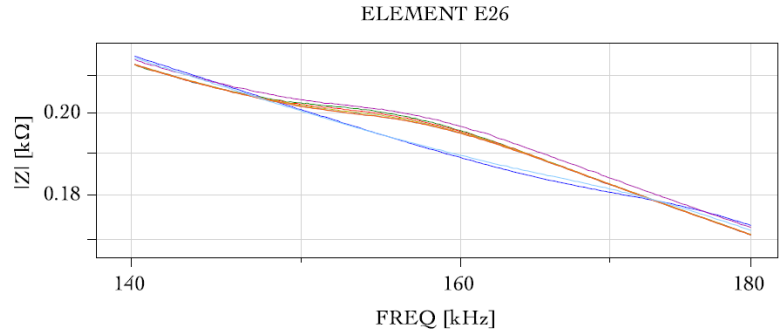
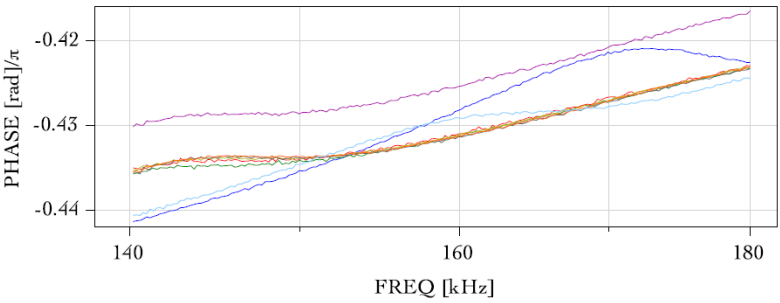
ELEMENT E24



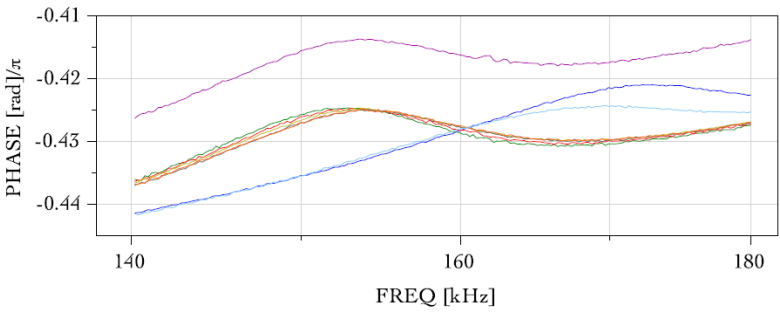
- E24, 06092020, Disk 2, 07/09/20,
- E24, 07112024, Disk 3, 07/11/20,
- E24, 07132024, Disk 5, 07/13/20,
- E24, 07152024, Disk 6, 07/15/20,
- E24, 07162024, Disk 7, 07/16/20,
- E24, 07192024, Disk 9, 07/19/20,
- E24, 07202024, Disk 10, 07/20/20
- E24, 07202064, Disk 13, 07/20/20



E25, 06092020, Disk 2, 07/09/20,
 E25, 07112025, Disk 3, 07/11/20,
 E25, 07132025, Disk 5, 07/13/20,
 E25, 07152025, Disk 6, 07/15/20,
 E25, 07162025, Disk 7, 07/16/20,
 E25, 07192025, Disk 9, 07/19/20,
 E25, 07202025, Disk 11, 07/20/20
 E25, 07202065, Disk 13, 07/20/20



E26, 06092020, Disk 2, 07/09/20,
 E26, 07112026, Disk 3, 07/11/20,
 E26, 07132026, Disk 5, 07/13/20,
 E26, 07152026, Disk 6, 07/15/20,
 E26, 07162026, Disk 7, 07/16/20,
 E26, 07192026, Disk 9, 07/19/20,
 E26, 07202026, Disk 11, 07/20/20
 E26, 07202066, Disk 13, 07/20/20



Appendix V - Radiation Damage of Electronics – Single Event Effects versus Cumulative Effects

In order to be able to develop effective and efficient test plans for radiation tolerance of components, it helps to understand what types of radiation effects occur in electronic components, and the radiation interaction mechanisms involved. The two main categories of radiation effects are called Single Event Effects (SEEs) and long-term or cumulative effects (CEs). These two main categories and their multiple subcategories are shown in Figure V.1.

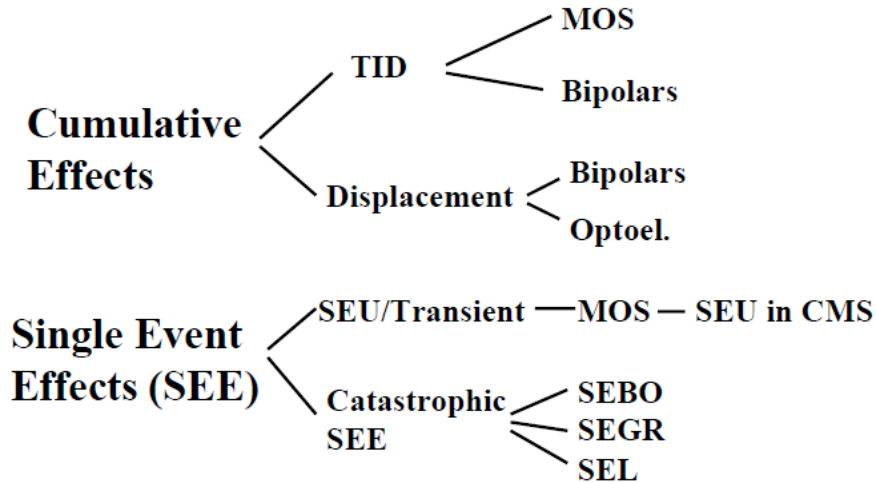


Figure V.1. Diagram of the two main categories of radiation effects, SEEs and long-term or CEs, and their multiple subcategories that include TID, displacement, transient and catastrophic effects.

SEEs are due to the energy deposited by one single charged particle as it passes through a semiconductor material in the electronic device. Therefore, a SEE can happen in any moment, and their probability is expressed in terms of cross-section. An electronic device that is sensitive to SEE can exhibit failure at any moment after beginning its operation in a radiation environment. On the contrary, CEs are gradual effects taking place during the whole lifetime of the electronics exposed in a radiation environment. A device sensitive to the Total Ionizing Dose (TID) or Displacement Damage will exhibit failure in a radiation environment when the accumulated TID (or particle fluence) has reached its tolerance limits. It is therefore, in principle, possible to foresee when the failure will happen for a given, well known and characterized component.

During the test irradiations, ionization effects will be induced by the ionization energy deposited by charged electrons and gamma-rays (even though gammas are not directly ionizing, they can induce ionizing energy depositions). The heart of TID effects is the energy deposition in silicon dioxide, because the electron-hole pairs created in this material do not completely recombine in a very short time. In the presence of an electric field in the oxide, a great amount of the pairs does not recombine, and both electrons and holes start to drift in the electric field. Electrons, with a much higher mobility, can easily leave the oxide. Holes instead can be trapped in defect centers in the oxide. Additionally, this process can create (or better activate) defects at the silicon-oxide interface. The charge buildup and the activation of defects are the two reasons for device degradation induced by TID. An example of the effects of relatively high radiation dose on a flash memory component is shown in Figure V.2.

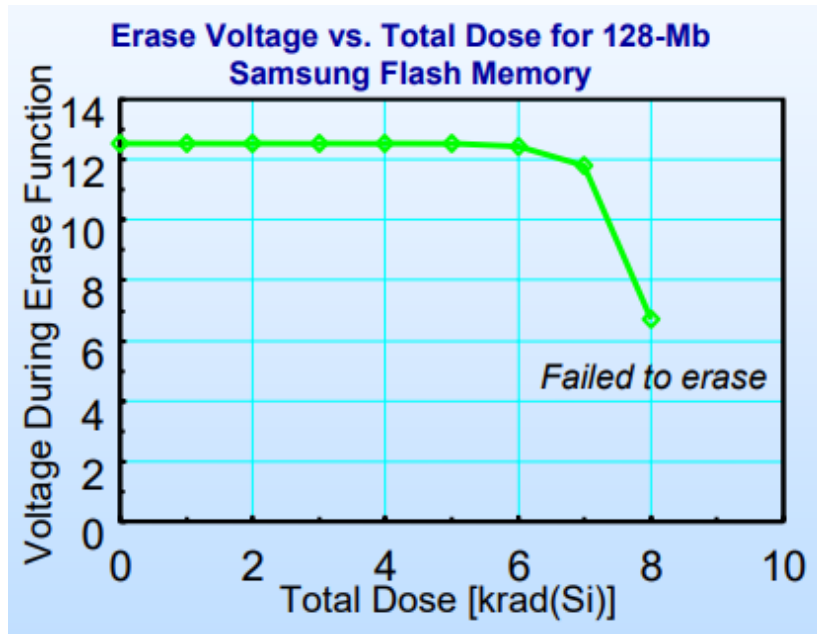


Figure V.2. An example of the effects of relatively high radiation dose on a flash memory component.

Pacific Northwest National Laboratory

902 Battelle Boulevard
P.O. Box 999
Richland, WA 99354
1-888-375-PNNL (7665)

www.pnnl.gov